JOURNAL
OF
GEOMAGNETISM
AND
GEOELECTRICITY

VOL. XI NO. 4

SOCIETY
OF
TERRESTRIAL MAGNETISM AND ELECTRICITY
OF
JAPAN

1960
KYOTO

JOURNAL OF GEOMAGNETISM AND GEOELECTRICITY

The fields of interest of this quarterly Journal are as follows:

Terrestrial Magnetism	Aurora and Night Airglow
Atmospheric Electricity	The Ozone Layer
The Ionosphere	Physical States of the Upper Atmosphere
Radio Wave Propagation	Solar Phenomena relating to the Above Subjects
Cosmic Rays	Electricity within the Earth

The text should be written in English, German or French. The price is set as 1 dollar per number.

The Editors

Fluid Motions in a Sphere IV

Thermal Instability of a Rotating Fluid Sphere Heated within under a Uniform Magnetic Field (2)

By Tomikazu NAMIKAWA

Institute of Polytechnics, Osaka City University

(Read May 18, 1958; Received March 25, 1960)

Abstract

The conditions for which a fluid sphere heated within and subject to the simultaneous action of a uniform magnetic field and rotation can become unstable via a marginal state of purely oscillatory motion are studied. Different from the results of the paper (Namikawa, 1957b), over-stability occurs both under astrophysical and terrestrial conditions.

1. Introductions

In earlier paper, (Namikawa, 1957c; this paper will be referred to hereafter as [1]) we studied the simultaneous effect of a uniform magnetic field and rotation on the thermal instability of a fluid sphere heated within.

However, the discussion was limited to the case when the principle of the exchange of stabilities is valid. We shall examine in this paper the possibility which the instability sets in as an increasing amplitude oscillation. This possibility was hnown to occur when rotation or a uniform magnetic field alone is present (Namikawa 1957 a, b).

It will be difficult to demonstrate the occurence of the over-stability or the ordinary cellular convection in a fluid sphere experimentally and compare the result with the theoretical predictions. However, this demonstration by experiment was done by Fultz and Nakagawa (1954–1957) in the case of thermal instability of a layer of fluid below, and it was in complete agreement with the theoretical predictions by Chandrasekhar (1952a–1956).

Thermal Instability of a fluid sphere was studied by Chandrasekhar (1952b), Backus (1955), and extent of these investigation to a rotating fuid sphere was carried out by Takeuchi and Shimazu (1954), Chandrasekhar (1957b) Bishop (1958) and Namikawa (1957a).

2. An Examination of the Principle of the Exchange of Stabilities

We shall start from eqn. (37) of paper [1]. This derivation is given briefly in the

appendex. The notations are the same as in [1], but for convenience the definitions are listed below.

ρ : density at the surface of sphere,
$\bar{\rho}$: mean density of sphere,
α : coefficient of volume expansion,
κ : thermometric conductivty,
μ : magnetic permeability,
σ : electrical conductivity,
η : $1/4\pi\mu\sigma$
a : radius of sphere,
β : adverse temperature gradient maintained,
g : acceleration due to gravity,
G : constant of gravitation,
γ : $4/3\pi\bar{\rho}G\alpha$
H : intensity of impressed magnetic field,
Ω : angular velocity of rotation,
λ : frequency of oscillation in case of overstability,
ω : λa^2
n : order of spherical harmonics,
m : degree of spherical harmonics,
R : $\dfrac{2\beta\gamma a^6}{\kappa\eta}$
R_c : critical value of R for the onset of instability,
T : $\dfrac{2\Omega}{\eta}a^2$
Q : $\dfrac{\mu^2H^2\sigma a^2}{p_0\eta}$

i) axially symmetric disturbance

We firstly examine axially symmetric disturbance.

In this case, eqn. (37) of [1] is reduced to the following form,

$$\left(\omega^2+\eta\alpha_j^2\omega+\frac{\eta^2\alpha_j^2}{5}Q\right)\left\{\omega^3+(\kappa+\eta)\alpha_j^2\omega^2+\kappa\eta\alpha_j^2\left(\alpha_j^2+\frac{Q}{5}\frac{\eta}{\kappa}-\frac{2}{\alpha_j^4}R\right)\omega\right.$$
$$\left.+\kappa\eta^2\alpha_j^4\left(\frac{Q}{5}-\frac{2}{\alpha_j^4}R\right)\right\}+\frac{\eta^2T^2}{5}(\omega+\kappa\alpha_j^4)(\omega+\eta\alpha_i^4)^2=0. \qquad (1)$$

This eqn. can be written as follows,

$$\omega^5+A\omega^4+B\omega^3+C\omega^2+D\omega+E=0, \qquad (2)$$

where

$$A=\kappa(1+2\delta)\alpha_j^2,$$
$$B=\kappa\eta_j^2\left\{(2+\delta)\alpha_j^2+\frac{2\delta}{5}Q+\frac{\delta}{5}\frac{T^2}{\alpha_j^2}-\frac{2}{\alpha_j^4}R\right\},$$

$$\left.\begin{aligned} C&=\kappa\eta^2\alpha_j^4\left\{\alpha_j^2+\frac{2(1+\delta)}{5}Q+\frac{(1+2\delta)}{5}\frac{T^2}{\alpha_j^2}-\frac{4}{\alpha_j^4}R\right\},\\ D&=\kappa\eta^3\alpha_j^4\left\{\frac{2\alpha_j^2}{5}Q+\delta\left(\frac{Q}{5}\right)^2+\frac{2+\delta}{5}T^2-\left(\alpha_j^2+\frac{Q}{5}\right)\frac{2}{\alpha_j^2}R\right\},\\ E&=\frac{\kappa\eta^4\alpha_i^6}{5}\left\{Q\left(\frac{Q}{5}-\frac{2}{\alpha_j^4}R\right)+T^2\right\}, \end{aligned}\right\} \qquad (3)$$

and

$$\delta=\frac{\eta}{\kappa}.$$

From the eqn. (2), it follows that if $E<0$, it admits a positive real root at least. $E<0$ is therefore a sufficient condition for the principle of the exchange of stabilities to be valid.

Therefore, let

$$E>0. \qquad (4)$$

This is a necessary condition for eqn. (2) does not allow positive roots and the corresponding solutions lead to an exponential damping of an initial disturbance.

We have to examine whether under these conditions the complex roots of (2) is able to have a positive real part. If x and y denote the real and imaginary part of a complex root of eqn. (2), they statisfy the equations,

$$(5x+A)y^4-(10x^3+6Ax^3+3Bx+C)y^2+x^5+Ax^4+Bx^3+Cx^2+Dx+E=0, \qquad (5)$$

and

$$y^4-(10x^2+4Ax+B)y^2+5x^4+4Ax^3+3Bx^2+2Cx+D=0. \qquad (6)$$

These are the second order algebraic eqns. for y^2; we get form (5) and (6) the next equations,

$$24x^5+24Ax^4+2(2A^2+7B)x^3+3(3AB+3C)x^2+2(AC+2D)x+AD-E=0, \qquad (7)$$

and

$$40x^3+24Ax^2+2(2A^2+B)x+AB-C=0. \qquad (8)$$

It is difficult to find the general conditions, under which the eqns. (7) and (8) have real positive root.

But, if $$B>0. \qquad (9)$$

the eqn. (8) admits a real positive root when,

$$AB-C<0. \qquad (10)$$

From (9) and (10) we get

$$C>0. \qquad (11)$$

If $$AD-E>0, \qquad (12)$$

making use of (4),
we have

$$D>0, \qquad (13)$$

and the eqn. (7) admits no real positive roots. Therefore, under the conditions (4) and (9), the eqns. (7) and (8) admit a real positive root when the inequalities (10) and (16) hold and by letting $AD-E$ and $AB-C\to 0$ through negative values, we shall have the case when a complex root of eqn. (2), having a positive real part, tends to a purely imaginary limit,

Therefore, if

$$E>0, \tag{14}$$

$$B>0, \tag{15}$$

$$AD-E<0, \tag{16}$$

and

$$AB-C<0, \tag{17}$$

the principle of the exchange of stabilities can not be applied and we shall have a case of overstability. According to (3), the conditions (14), (15), (16), and (17), are equivalent to

$$\frac{Q}{5}+\frac{T^2}{Q}>\frac{2}{a_j^4}R, \tag{18}$$

$$(2+\delta)a_j^2+\frac{2\delta}{5}Q+\frac{\delta}{5}\frac{T^2}{a_j^2}>\frac{2}{a_j^4}R, \tag{19}$$

$$\left\{2(1+2\delta)a_j^2+\frac{2\delta^2}{5}Q\right\}\frac{Q}{5}+\frac{2(1+\delta)^2}{5}T^2<\left\{\frac{1+\delta}{5}Q+(1+2\delta)a_j^2\right\}\frac{2}{a_j^4}R, \tag{20}$$

and

$$2(1+\delta)^2a_j^2+\frac{2\delta^2}{5}Q<\frac{2}{a_j^4}R, \tag{21}$$

The inequalities (18), (19), (20), and (21), can be combined in the form,

$$\frac{Q}{5}+\frac{T}{Q}>\frac{2}{a_j^4}R>\frac{\left\{2(1+2\delta)a_i^2+\frac{2\delta^2}{5}Q\right\}\frac{Q}{5}+\frac{2(1+\delta)^2}{5}T^2}{(1+2\delta)a_j^2+\frac{1+\delta}{5}Q}, \tag{22}$$

$$\frac{Q}{5}+\frac{T^2}{Q}>\frac{2}{a_j^4}R>2(1+\delta)^2a_j^2+\frac{2\delta^2}{5}Q, \tag{23}$$

$$(2+\delta)a_j^2+\frac{2\delta}{5}Q+\frac{\delta}{5}\frac{T^2}{a_j^2}>\frac{2}{a_j^4}R>\frac{\left\{2(1+2\delta)a_j^2+\frac{2\delta^2}{5}Q\right\}\frac{Q}{5}+\frac{2(1+\delta^2)}{5}T^2}{(1+2\delta)a_j^2+\frac{1+\delta}{5}Q} \tag{24}$$

$$(2+\delta)a_j^2+\frac{2\delta}{5}Q+\frac{\delta}{5}\frac{T^2}{a_j^2}>\frac{2}{a_j^4}R>2(1+\delta)^2a_j^2+\frac{2\delta^2}{5}Q, \tag{25}$$

We can rearrange the outer inequalities of (22), (23), (24), and (25) to give,

$$5(5T^2-Q^2)a_j^2+Q\{(1-\delta)Q^2-5(1+\delta)T^2\}>0, \tag{26}$$

$$-10(1+\delta)^2Qa_j^2+5T^2+(1-2\delta^2)Q^2>0, \tag{27}$$

$$25(2+\delta)(1+2\delta)a_j^6+5\delta(5\delta+1)a_j^4Q+\{2\delta Q^2-5(3\delta+2)T^2\}+\delta(1+\delta)QT^2>0, \tag{28}$$

$$-5(2\delta+3)a_j^4+2(1-\delta)a_j^2Q+T^2>0\,. \tag{29}$$

These four eqns. are the necessary conditions for instability to arise through oscillation of increasing amplitude; it is therefore the conditions for the principle of the exchange of stabilities not be valid.

If $T=0$ in these eqns,

$$\delta>1 \tag{30}$$

becomes a sufficient condition for the principle of the exchange of stabilities to be valid and this is equal to the inequality (63) of the paper (Namikawa, 1957b). But, for $T\neq 0$, we have no simple condition as (30) for the principle of the exchange of stabilities to be valid and the overstability is able to arise even if $\delta>1$.

When the conditions (26)–(29) are satisfied, we have a case of overstability, then the frequency of oscillation at marginal stability will be given by from (5) and (6)

$$\lambda=\sqrt{\frac{B\pm\sqrt{B^2-4D}}{2}}\Big/a^2 \tag{31}$$

and the critical value of R for the onset of the overstability can be obtained, letting $AB-C\to 0$ $AD-E\to 0$, as follows,

$$R_c^0=a_1^4\frac{\left\{(1+2\delta)a_1^2+\frac{\delta^2}{5}Q\right\}\frac{Q}{5}+\frac{(1+\delta)^2}{5}T^2}{(1+2\delta)a_1^2+\frac{1+\delta}{5}Q}=a_1^4\left\{(1+\delta)^2+\frac{\delta^2}{5}Q\right\}, \tag{32}$$

where a_1 is the first root of the eqn. $J_{n+1/2}(a_j)=0$.

We can find a relation between Q and T from (32)

$$\frac{\delta^3}{5(1+\delta)^2}Q^2+\frac{\delta(3\delta+1)}{1+\delta}a_1^2Q+5(1+2\delta)a_1^4-T^2=0\,. \tag{33}$$

This eqn. means that purely oscillatory motion occurs at a fixed value of angular velocity of a sphere for a given intensity of applied magntic field or vice versa.

Solving eqn, (33) of Q, we find

$$Q=\frac{5(1+\delta)^2}{2\delta^3}a_1^2\left[-\frac{\delta(3\delta+1)}{1+\delta}\pm\sqrt{\left\{\frac{\delta(3\delta+1)}{1+\delta}\right\}^2-\frac{4}{5}\frac{\delta^3}{(1+\delta)^2}\left\{5(1+2\delta)-\frac{T^2}{a_1^4}\right\}}\right] \tag{34}$$

Therefore, the next inequality,

$$5(1+2\delta)a_1^4-T^2<0 \tag{35}$$

is a necessary condition for Q is real positive.

ii) asymmetric disturbance

In the case of axially asymmetric disturbances, (37) of [1] is reduced to the next form

$$\left[\omega^2+\eta\left\{a_i^2-\frac{inT}{(n+1)(n+2)}\right\}\omega+\eta^2a_j^2\left\{\frac{n\{(n+2)^3+n(2n+3)\}}{(n+1)^2(n+2)^2(2n+3)}-\frac{in\bar{T}}{(n+1)(n+2)}\right\}\right]$$
$$\times\left[\omega^3+\kappa\left\{(1+\delta)a_j^2-\frac{iT}{n+1}\delta\right\}\omega^2+\kappa\eta a_j^2\left\{a_j^2+\frac{(3n+5)\delta}{(n+1)^2(2n+3)}Q-\frac{n(n+1)}{a_j^4}R\right.\right.$$

$$-\frac{iT}{n+1}(1+\delta)\Big\}\omega+\kappa\eta^2\alpha_j^4\Big\{\frac{(3n+5)}{(n+1)^2(2n+3)}Q-\frac{n(n+1)}{\alpha_j^4}R-\frac{iT}{n+1}\Big\}\Big]$$
$$+\frac{n(n+2)}{(n+1)^2(2n+3)}T^2\eta^2(\omega+\kappa\alpha_j^2)\Big\{\omega+\eta\alpha_j^2+\frac{2i\eta\alpha_j^2}{n+2}\frac{Q}{T}\Big\}^2=0 \qquad (36)$$

We can write the above eqn, (36) as follows

$$\omega^5+(A_1-iA_2)\omega^4+(B_1-iB_2)\omega^3+(C_1-iC_2)\omega^2+(D_1-iD_2)\omega+E_1-iE^2=0\,, \qquad (37)$$

where

$$A_1=\kappa(1+2\delta)\alpha_j^2\,,$$
$$A_2=\frac{2\eta T}{n+2}$$
$$B_1=\kappa\eta\alpha_j^2\Big[(2+\delta)\alpha_j^2+\frac{(3n+5)(n+2)^2+n\{(n+2)^3+n(2n+3)\}}{(n+1)^2(n+2)^2(2n+3)}\delta Q+\frac{n\delta T^2}{(n+2)(2n+3)}$$
$$-\frac{n(n+1)}{\alpha_j^4}R\Big]\,,$$
$$B_2=2\kappa\eta\alpha_j^2\frac{(1+2\delta)}{(n+2)}T=A_1A_2$$
$$C_1=\kappa\eta^2\alpha_j^4\Big[\alpha_j^2+\frac{n\{(n+2)^3+n(2n+3)\}+(3n+5)(n+2)^2}{(n+1)^2(2n+3)(n+2)^2}(1+\delta)Q+\frac{n(1+2\delta)}{(n+2)(2n+3)}\frac{T^2}{\alpha_j^4}$$
$$-\frac{2n(n+1)}{\alpha_j^4}R\Big]\,,$$
$$C_2=\frac{\kappa\eta^2\alpha_j^2nT}{(n+1)(n+2)}\Big[\frac{2(n+1)(2+\delta)}{n}\alpha_j^2$$
$$+\frac{n\{(n+2)^3+n(2n+3)\}+(3n+5)(n+2)-4(n+2)^2n(n+1)}{n(n+1)^2(n+2)(2n+3)}\delta Q-\frac{n(n+1)}{\alpha_j^4}R\Big]\,,$$
$$D_1=\kappa\eta^3\alpha_j^4\Big[\frac{n\{(n+2)^3+n(2n+3)\}+(3n+5)(n+2)^2}{(n+1)^2(n+2)^2(2n+3)}\alpha_j^2Q$$
$$+\frac{n\{(3n+5)(n+2)^3+n(3n+5)(2n+3)-4(n+1)^2(n+2)}{(n+1)^4(n+2)^2(2n+3)^2}\delta Q^2+\frac{n(2+\delta)}{(n+2)(2n+3)}T^2$$
$$-\Big\{\alpha_j^2+\frac{n\{(n+2)^3+n(2n+3)\}}{(n+1)^2(n+2)^2(2n+3)}Q\Big\}\frac{n(n+1)}{\alpha_j^4}R\Big]\,, \qquad (38)$$
$$D_2=2\kappa\eta^3\alpha_j^4\frac{nT}{(n+1)(n+2)}\Big[\frac{n+1}{n}\alpha_j^4+\frac{(n+2)(3n+1)+(n+2)^3+n(2n+3)}{2(n+1)^2(n+2)(2n+3)}(1+\delta)Q$$
$$-\frac{n(n+1)}{\alpha_j^4}R\Big]\,,$$
$$E_1=\kappa\eta^4\alpha_j^6\Big[\frac{n(3n+5)\{(n+2)^3+n(2n+3)\}-4n(n+1)^2(n+2)(2n+3)}{(n+1)^4(n+2)^2(2n+3)^2}Q^2+\frac{nT^2}{(n+1)(2n+3)}$$
$$-\frac{n\{(n+2)^3+n(2n+3)\}}{(n+1)^2(n+2)^2(2n+3)}Q-\frac{n(n+1)}{\alpha_j^4}R\Big]\,,$$

and

$$E_2=\frac{nT}{(n+1)(n+2)}\Big[\frac{(n+2)(3n+5)+(n+2)^3+n(2n+3)-4(n+2)^2(n+1)}{(n+1)^2(n+2)(2n+3)}Q-\frac{n(n+1)}{\alpha_j^4}R\Big].$$

When ω is *a* real number x, eqn. (37) is written in the forms

$$x^5+A_1x^4+B_1x^3+C_1x^2+D_1x+E_1=0\,, \qquad (39)$$

and

$$A_2x^4+B_2x^3+C_2x^2+D_2x+E_2=0\,. \tag{40}$$

As A_2 is positive and E_2 is negative, eqn. (39) and (40) admits a positive real root at least when

$$E_1<0\,. \tag{41}$$

Therefore $E_1<0$ is a sufficient condition for the eqn. (37) has the real positive roots and the disturbance exponentially increases with time. There is no steady state, as E_2 is always negative for all values of n, Q and R.

$$E_1>0\,, \tag{42}$$

is a necessary condition for the eqn. (37) does not allow positive roots. The complex roots of eqn. (37) must satisfy the next two eqns. where x and y are the real and imaginary part of complex roots.

$$\begin{aligned}&x^5+A_1x^4-(10y^2-4A_2y-B_1)x^3-(6A_1y^2-3B_2y-C_1)x^2\\&+(5y^4-4A_2y^3-C_1y^2+D_2y+D_1)x+A_1y^4-B_2y^3-C_1y^2+D_2y+E_1=0\,,\end{aligned} \tag{43}$$

and

$$\begin{aligned}&(5y-A_2)x^4+4(A_1y-B_2)x^3-(10y^3-6A_2y^2-3B_1y+C_2)x^2\\&-(4A_1y^3-3B_2y^2-2C_1y+D_2)x+y^5-A_2y^4-B_1y^3+C_2y^2+D_1y-E_2=0\,.\end{aligned} \tag{44}$$

It is very difficult to examine whether the eqns. (43) and (44) are able to have real positive x under the conditions (42). If $x=0$, we have purely imaginary roots of eqns. (37), which satisfy the next eqns.

$$A_1(y^4-A_2y^3)-C_1y^2+D_2y+E_1=0\,. \tag{45}$$

and

$$y^5-A_2y^4-B_1y^3+C_2y^2+D_1y-E_2=0\,. \tag{46}$$

As the eqn. (45) is a fourth order algedraic eqn. it can be solved algebraically.

Therefore we can get the value of R replacing in (46) with the value of y obtained by solving (45). But it is troublesome, so we shall return to it in another paper. We discuss only axially symmetric case hereafter.

3. Examination of Onset of Instability in the Axially Symmetric Case

From (33), we find that the overstability occurs along the line, expressed by the eqn. (33), in the (T, Q) plane. The critical value of R for the onset of ordieary cellular convection is found, letting $E\to 0$, (cf. paper. [1]).

$$R_c^{\text{con}}=\frac{\alpha_1^4}{2}\left(\frac{Q}{5}+\frac{T^2}{Q}\right). \tag{47}$$

In order to examine the intersection of R_c^{con} and R_c^0 curves we must insert the relation (33) in (47), thus we have

$$R_c^{\text{con}}=\frac{\alpha_1^4}{2}\left\{\frac{(1+\delta)^2+\delta^3}{5(1+\delta)^2}Q+\frac{\delta(3\delta+1)}{1+\delta}\alpha_1^2+\frac{5(1+2\delta)\alpha_1^4}{Q}\right\}. \tag{48}$$

This has a minimum at

$$Q=Q_m=5(1+\delta)\alpha_1^2\sqrt{\frac{1+2\delta}{\delta^3+(1+\delta)^2}}\,. \tag{49}$$

From the eqns. (32) and (48), we get next eqn. which is satisfied by the intersecting point Q^* of the R_c^{con} and R_c^0 curves.

$$\{(1+\delta)^2(1-2\delta^2)+\delta^3\}Q^{*2}+5(1+\delta)\{\delta(3\delta+1)-2(1+\delta)^3\}\alpha_1^2Q^*+25(1+\delta)^2(1+2\delta)\alpha_1^4=0\,. \tag{50}$$

The roots of the eqn. (50) are

$$Q^*=\frac{5(1+\delta)\alpha_1^2}{2f_1(\delta)}\left[f_2(\delta)\pm\sqrt{(1+2\delta)f_3(\delta)}\right], \tag{51}$$

where

$$\left.\begin{aligned} &f_1(\delta)\equiv(1+\delta)^2(1-2\delta^2)+\delta^3=-2\delta^4-3\delta^3-\delta^2+2\delta+1\,,\\ &f_2(\delta)\equiv-\delta(3\delta+1)+2(1+\delta)^3=(2\delta+1)(\delta^2+\delta+2)>0\\ \text{and}\quad &f_3(\delta)\equiv(2\delta+1)(\delta^2+\delta+2)^2-4(-2\delta^4-3\delta^3-\delta^2-2\delta+1)=\delta(2\delta^4+13\delta^3+24\delta^2+17\delta+4)>0 \end{aligned}\right\} \tag{52}$$

From (52), we can see that the value of Q, at the intersecting point, $Q^*(>0)$, of R_c^{con} and R_c^0 curves depends on the sign of $f_1(\delta)$.

f_1 has a real positive root $\delta_1(\fallingdotseq 0.8)$ for $\frac{1}{2}<\delta<1$.

i) $f_1>0$, for $0<\delta<\delta_1$ and R_c^{con} and R_c^0 curves intersect at two points.

The convection curve starts on the R_c — axis at the point

$$R_c^{\text{con}}\to\infty \qquad (Q\to 0)\,, \tag{53}$$

and for $Q\to\infty$ becomes asymptotic to the line

$$R_c^{\text{con}}=\frac{\alpha_1^4\{(1+\delta)^2+\delta^3\}}{10(1+\delta)^2}Q \qquad (Q\to\infty)\,. \tag{54}$$

On the other hand, the over-stability curve starts on the R_c — axis at

$$R_c^0=\alpha_1^6(1+\delta)^2\,, \quad (Q=0) \tag{55}$$

and for $Q\to\infty$ becomes asymptotic to the line

$$R=\frac{\delta^2\alpha_1^4}{5}Q \qquad (Q\to\infty)\,. \tag{56}$$

It follows that starting beneath the convection curve, the over-stability curve intersects at

$$Q_1^*=\frac{5(1+\delta)\alpha_1^2}{2f_1}\left[f_2-\sqrt{(1+2\delta)f_3}\right], \tag{57}$$

with the convection curve, lies above the convection curve for

$$Q_1^*<Q<Q_2^*=\frac{5(1+\delta)\alpha_1^2}{2f_1}\left[f_2+\sqrt{(1+2\delta)f_3}\right], \tag{58}$$

and again lies beneath the convection curve for

$$Q>Q_2^*. \tag{59}$$

This means that arising as the over-stabillity for $Q<Q_1^*$, the thermal instability arises as the ordinary cellular convection for $Q_1^*<Q<Q_2^*$ and again arises as the over-stability for $Q>Q_2^*$; this is what happens under astrophysical conditions ($\delta<1$).

ii) $f_1=0$, for $\delta=\delta_1$ and the over-stability curve, staring beneath the convection curve, intersects at

$$Q_3^*=\frac{5(1+\delta)\alpha_1^2}{\delta^2+\delta+2}, \tag{60}$$

with the convection curve, lies adove the covection curve for $Q>Q_3^*$, and becomes asymtotic to the convection curve. This means that the instsbility, arising as the over-stability for $Q<Q_3^*$, arises as the ordinary cellular convection for $Q>Q_3^*$ and the over-stability and the convection occurs at the same time for the large value of Q.

iii) $f_1<0$, for $\delta>\delta_1$ and the over-stability curve, starting beneath the convction curve, intersects at

$$Q_4^*=\frac{5(1+\delta)\alpha_1^2}{2f_1}\left[f_2-\sqrt{(1+2\delta)f_3}\right], \tag{61}$$

and lies above the convection curve for $Q>Q_4^*$.

This means that the instability, arising as the over-stability for $Q<Q_4^*$ and arises as the ordinary convection for $Q>Q_4^*$.

This is what happens under normal terrestrial conditions ($\delta>1$).

iv) The two extreme conditions $\delta\to 0$ and $\delta\to\infty$.

For $\delta\to 0$, two curves become asymptotic to the lines

$$R_c^{\mathrm{con}}=\frac{\alpha_1^4}{2}\left\{\frac{Q}{5}+\frac{5\alpha_1^4}{Q}\right\}, \tag{62}$$

and

$$R_c^0=\alpha_1^6(1+\delta)^2. \tag{63}$$

Two intersecting points are determined from the eqn.

$$Q^{*2}-10\alpha_1^2Q^*+25\alpha_1^4=0, \tag{64}$$

and

$$Q^*=5\alpha_1^2. \tag{65}$$

This is equal to the expression (49) ($\delta=0$). We find that when $\delta\to 0$, instability always arises as the over-stability except at $Q^*=5\alpha_1^2$.

For $\delta\to\infty$, the two curves become asymptotic to the lines

$$R_c^{\mathrm{con}}=\frac{\delta\alpha_1^4}{2}\left(\frac{Q}{5}+3\alpha_1^2+\frac{10\alpha_1^4}{Q}\right), \tag{66}$$

and

$$R_c^0=\delta^2\alpha_1^4\left(\alpha_1^2+\frac{Q}{5}\right), \tag{67}$$

and the value of Q at intersecting point tends to zero.

In this case, the istability always as the ordinary convection.

4. Concluding Remarks

We examined in the paper [1] and in this paper the manner of the onset of thermal instability of a fluid sphere under the simultaneous action of a magnetic field and rotation. On accound of the mathematical difficulities in calculation, only the axially symmetric instability was studied in detail.

In paper [1], assuming the validity of the principle of exchange of stabilities, we studied only the steady convection, while in this paper we examined the principle of exchange of stabilities and studied a marginal state of purely oscillatory motions.

No simple sufficient condition as the inequality (63) in the paper (Namikawa, 1957b), $\delta>1$, can be obtained, so we have a case of over-stability both in the astrophysical conditions ($\delta<1$) and in the terrestrial conditions ($\delta>1$). A marginal state of purely oscillatory motion does not occur at arbitrary values of Q and T and does at a fixed value of angular velocity of a sphere for a given intensity of the applied magnetic field or vice versa.

The convection curve has a minimum at the value of Q given by (49), while the over-stability curve is a monotoneous increasing with Q. In the case of the paper (Namikawa, 1957b), the over-stability curve always starts above the convection curve, but in the case of this paper the convection curve always starts above the over-stability curve. This meavs that the over-stability occurs at the small value of Q.

a) When $\frac{\eta}{\kappa}<\delta\fallingdotseq 0.8$, the over-stbility occurs at the small ($Q<Q_1^*$) or at the large ($Q>Q_2^*$) values of Q, while the ordinary convection arises for the moderate values of Q given by (58). Under astrophysical condition, for example, in the so called hydrogen-convection zone in the solar atmosphere (Chandrasekhar, 1952a) $\kappa\sim 10^{13}\mathrm{cm}^2/\mathrm{sec}$, $\eta\sim 7\times 10^6\mathrm{cm}^2/\mathrm{sec}$ and $\delta\sim 7\times 10^{-7}\ll 1$.

This is the case above mentioed.

b) When $\frac{\eta}{\kappa}\geqslant\delta_1$, the over-stability occurs for the values of Q, given by (60) or (61) and for the larger values of Q, the ordinary convection occurs.

Under terrestrial conditions, for example, for mercury,

We have

$$\kappa=4.45\times 10^{-2}\mathrm{cm}^2/\mathrm{sec},\ \eta=7.6\times 10^3\mathrm{cm}^2/\mathrm{sec},\ \text{and}\quad \delta\sim 10^5\gg 1\,.$$

In the Earth's core (Bullard, 1954), we have

$$\kappa\sim 6\times 10^{-2}\,\mathrm{cm}^2/\mathrm{sec},\ \eta\sim 2.7\times 10^4\,\mathrm{cm}^2/\mathrm{sec},\ \text{and}\quad \delta\sim 4.5\times 10^5\gg 1\,.$$

As Q^* (the value of Q at the intersecting point of the over-stability curve and the convection curve) is very small, we may say, in mercury at the room temperature or in the Earth's core, thermal instability arises as the ordinary steady convection.

But, because of the existence of the strong Toroidal magnetic field in the Earth's core, (Bullard, 1948) it is hoped to examine thermal instability under Toroidal magnetic

field.

Recently, Rikitake (1959 a, b) studied thermo-magneto-hydrodynamic oscillation in the Earth's core under the steady Poroidal and Toroidal magnetic field. He got twenty years for the period of the oscillation, which is in accordance with that of a part of the geomagnetic secular variations.

5. Appendix

1. Equation of motion

A brief derivation of the eqn. (1) is given below.

Consider a homogeneous electrical conducting fluid sphere of radius a rotating with an angular velocity about Z-axis under a uniform magnetic field, the direction of which is parallel to Z-axis. A heat generating source is supposed. The rate of heat generation is assumed such that in the absence of conduction and convection the temperature would rise at a uniforme rate ϵ. The equation of motion, of Maxwell, and of heat conduction appropriate to the problem on hand are

$$\rho\frac{\partial \boldsymbol{u}}{\partial t}+\rho(\boldsymbol{u}\cdot\nabla)\boldsymbol{u}=-\nabla p+2\rho\boldsymbol{u}\times\boldsymbol{\Omega}+\rho\nu\nabla^2\boldsymbol{u}+\rho\nabla V+\mu\boldsymbol{j}\times\boldsymbol{H}, \tag{A. 1}$$

$$\frac{\partial \rho}{\partial t}+\mathrm{div}(\rho\boldsymbol{u})=0, \tag{A. 2}$$

$$\mathrm{curl}\ \boldsymbol{H}=4\pi\boldsymbol{j}, \tag{A. 3}$$

$$\mathrm{curl}\boldsymbol{E}=-\mu\frac{\partial \boldsymbol{H}}{\partial t}, \tag{A. 4}$$

$$\mathrm{div}\ \boldsymbol{H}=0, \tag{A. 5}$$

$$\mathrm{div}\ \boldsymbol{E}=4\pi c^2 q, \tag{A. 6}$$

$$\boldsymbol{j}=\sigma(\boldsymbol{E}+\boldsymbol{u}\times\boldsymbol{H}), \tag{A. 7}$$

$$\frac{\partial T}{\partial t}+(\boldsymbol{u}\cdot\nabla)T=\kappa\nabla^2 T+\epsilon, \tag{A. 8}$$

where ρ, $\boldsymbol{u}$, p, $\boldsymbol{\Omega}$, ν, V, μ, $\boldsymbol{j}$, $\boldsymbol{H}$, $\boldsymbol{E}$, c, q, σ, T and κ are density, velocity, pressure, angular velocity of sphere, kinematic viscosity, gravitational potential, magnetic permeability, electric current density, magnetic field, electric field, velocity of light, electrical charge, electrical conductiuity, temperature and thermal diffccsivity respectively. We are here adopting the electromagnetic system of units.

The equations governing small departures from the stationary state are (cf. Namikawa 1957 a, b, c),

$$\frac{\partial \theta}{\partial t}=\kappa\nabla^2\theta+2\beta(ru_r), \tag{A. 9}$$

$$\frac{\partial \boldsymbol{u}}{\partial t}=-\frac{1}{\rho_0}\nabla p+2\boldsymbol{u}\times\boldsymbol{\Omega}+\gamma\theta\boldsymbol{r}+\frac{\mu H}{4\pi\rho_0}\frac{\partial \boldsymbol{h}}{\partial z}+\nu\nabla^2\boldsymbol{u}, \tag{A.10}$$

$$\frac{\partial \boldsymbol{h}}{\partial t}=H\frac{\partial \boldsymbol{u}}{\partial z}+\eta\nabla^2\boldsymbol{h}, \tag{A.11}$$

and

$$\mathrm{div}\ \boldsymbol{u}=\mathrm{div}\boldsymbol{h}=0, \tag{A.12}$$

where θ and $\boldsymbol{h}$ are perturbation in temperature and magnetic field.

Taking the curl of eqns. (A.10) and (A.11), we get

$$\frac{\partial \boldsymbol{\omega}}{\partial t}=\gamma\nabla\theta\times\boldsymbol{r}+2\Omega\frac{\partial \boldsymbol{u}}{\partial z}+\frac{\mu H}{4\pi\rho_0}\frac{\partial}{\partial z}\mathrm{curl}\boldsymbol{h}+\nu\nabla^2\boldsymbol{\omega}\,, \tag{A.13}$$

and

$$\frac{\partial}{\partial t}\mathrm{curl}\boldsymbol{h}=H\frac{\partial \boldsymbol{\omega}}{\partial z}+\eta\nabla^2(\mathrm{curl}\boldsymbol{h})\,. \tag{A.14}$$

Again taking the curl of eqn. (A.13), we have

$$-\frac{\partial}{\partial t}(\nabla^2\boldsymbol{u})=\gamma\mathrm{curl}(\nabla\theta\times\boldsymbol{r})-\frac{\mu H}{4\pi\rho^0}\frac{\partial}{\partial z}\nabla^2\boldsymbol{h}-\nu\nabla^4\boldsymbol{u}\,, \tag{A.15}$$

where $\boldsymbol{\omega}=\mathrm{curl}\boldsymbol{v}$.

Multiplying eqns. (A.11) (A.13) (A.14) and (A.15) by $\boldsymbol{r}$, we get

$$\frac{\partial}{\partial t}(rh_r)=H\boldsymbol{r}\frac{\partial \boldsymbol{h}}{\partial z}+\eta\nabla^2(rh_r)\,, \tag{A.16}$$

$$\frac{\partial}{\partial t}(r\omega_r)=2\Omega\boldsymbol{r}\frac{\partial \boldsymbol{u}}{\partial z}+\frac{\mu H}{4\pi\rho_0}\boldsymbol{r}\frac{\partial}{\partial z}(\mathrm{curl}\boldsymbol{h})+\nu\nabla^2(r\omega_r)\,, \tag{A.17}$$

$$\frac{\partial}{\partial t}(\mathrm{curl}\boldsymbol{h})_r=H\boldsymbol{r}\frac{\partial \boldsymbol{\omega}}{\partial z}+\eta\nabla^2 r(\mathrm{curl}\boldsymbol{h})_r\,, \tag{A.18}$$

and

$$-\frac{\partial}{\partial t}\nabla^2(ru_r)=\gamma L^2\theta+2\Omega\boldsymbol{r}\frac{\partial \boldsymbol{\omega}}{\partial z}-\frac{\mu H}{4\pi\rho_0}\boldsymbol{r}\frac{\partial}{\partial z}\nabla^2\boldsymbol{h}-\nu\nabla^4(ru_r)\,, \tag{A.19}$$

where

$$L^2=-\left(\frac{1}{\sin\theta}\frac{\partial}{\partial\theta}\sin\theta\frac{\partial}{\partial\theta}+\frac{1}{\sin^2\theta}\frac{\partial^2}{\partial\varphi^2}\right).$$

We express the velocity field and the magnetic field as a superposition of a poroidal and a toroidal vector in terms of four scalars.

$$\boldsymbol{u}=\nabla V\times\boldsymbol{I}_r+\mathrm{curl}(\nabla U\times\boldsymbol{I}_r) \tag{A.20}$$

$$\boldsymbol{h}=\nabla T\times\boldsymbol{I}_r+\mathrm{curl}\ (\nabla S\times\boldsymbol{I}_r) \tag{A.21}$$

where $\boldsymbol{I}_r$ is the unit vector of radius direction.

Five scalars U, V, T, S and θ are expressed as follows

$$\left.\begin{aligned} &U=\sum_{n,m}U_n^m(r,t)Y_n^m\,,\quad V=\sum_{n,m}V_n^m(r,t)Y_n^m\,,\\ &S=\sum_{n,m}S_n^m(r,t)Y_n^m\,,\quad T=\sum_{n,m}T_n^m(r,t)Y_n^m\,,\\ \text{and}\quad &\theta=\sum_{n,m}(r,t)Y_n^m\,, \end{aligned}\right\} \tag{A.22}$$

where Y_n^m is a surface spherical harmonic.

Operating Y_n^m to eqns. (A.9) (A.16) (A.17) (A.18) and (A.19) and executing the integration with respect to θ and φ, we get

$$a^2\frac{\partial}{\partial t}\Theta_n^m-\kappa\frac{1}{r^2}\left\{\frac{d}{dr}\left(r^2\frac{d}{dr}\right)-n(n+1)\right\}\Theta_n^m-2\beta an(n+1)\frac{U_n^m}{r}=0\,, \tag{A.23}$$

$$a^2\frac{\partial}{\partial t}n(n+1)\frac{S_n^m}{r}-\gamma n(n+1)\frac{1}{r^2}\left\{\frac{d}{dr}\left(r^2\frac{d}{dr}\right)-n(n+1)\right\}\frac{S_n^m}{r}$$
$$-Ha\left[\frac{(n-1)(n+1)(n-m)}{2n-1}r^{n-1}\frac{d}{dr}\left(r^{-n}U_n^m\right)\right.$$
$$\left.+\frac{n(n+2)(n+m+1)}{2n+3}r^{-(n+2)}\frac{d}{dr}(r^{n+1}U_{n+1}^m)+im\frac{V_n^m}{r^2}\right]=0\,, \tag{A.24}$$

$$a^2\frac{\partial}{\partial t}n(n+1)\frac{V_n^m}{r^2}-\nu n(n+1)\frac{1}{r^2}\left\{\frac{d}{dr}\left(r^2\frac{d}{dr}\right)-n(n+1)\right\}\frac{V_n^m}{r^2}$$
$$-\frac{Ha}{4\pi\rho_0}\left[\frac{(n-1)(n+1)(n-m)}{2n-1}r^{n-1}\frac{d}{dr}(r^{-n}T_{n-1}^m)\right.$$
$$\left.+\frac{n(n+1)(n+m+1)}{2n+3}r^{-(n+2)}\frac{d}{dr}\left(r^{n+1}\frac{T_{n+1}^m}{r}\right)-\frac{im}{r}\left\{\frac{d^2}{dr^2}-\frac{n(n+1)}{r^2}\right\}S_n^m\right]=0\,, \tag{A.25}$$

$$-n(n+1)a^2\frac{\partial}{\partial t}\frac{1}{r^2}\left\{\frac{d}{dr}\left(r^2\frac{d}{dr}\right)-n(n+1)\right\}\frac{U_n^m}{r}+\nu n(n+1)\left[\frac{1}{r^2}\left\{\frac{d}{dr}\left(r^2\frac{d}{dr}\right)\right.\right.$$
$$\left.\left.-n(n+1)\right\}\right]^2\frac{U_n^m}{r}+\frac{\mu Ha}{4\pi\rho_0}\frac{1}{r^2}\left\{\frac{d}{dr}\left(r^2\frac{d}{dr}\right)\right.$$
$$\left.-n(n+1)\right\}\left[\frac{(n-1)(n+1)(n-m)}{2n-1}r^{n-1}\frac{d}{dr}(r^{-n}S_{n-1}^m)\right.$$
$$\left.+\frac{n(n+2)(n+m+1)}{2n+3}r^{-(n+2)}\frac{d}{dr}(r^{n+1}S_{n+1}^m)+im\frac{T_n^m}{r^2}\right]-\gamma n(n+1)a^5\Theta_n^m=0\,, \tag{A.26}$$

and

$$a^2\frac{\partial}{\partial t}n(n+1)\frac{T_n^m}{r^2}-\gamma n(n+1)\frac{1}{r^2}\left\{\frac{d}{dr}\left(r^2\frac{d}{dr}\right)-n(n+1)\right\}\frac{T_n^m}{r^2}$$
$$-Ha\left[\frac{(n-1)(n+1)(n-m)}{2n-1}r^{n-1}\frac{d}{dr}(r^{-n}V_{n-1}^m)+\frac{n(n+2)(n+m+1)}{2n+3}r^{-(n+2)}\frac{d}{dr}(r^{n+1}V_{n+1}^m)\right.$$
$$\left.-im\frac{1}{r}\left\{\frac{d^2}{dr^2}-\frac{n(n+1)}{r^2}\right\}U_n^m\right]=0\,, \tag{A.27}$$

where length is measured by unit of a, radius of sphere.

These five eqns. are the basic equation of this problem.

2. Boundary conditions

As is in the previous papers (Namikawa, 1957 a, b, c), we shall treat basic eqns. neglecting the viscus term, The boundary conditions are the vanishing of perturbation in temperature, of radius component of velocity, and continuity of magnetic field and of tangential compnent of electric field on the boundary surface.

3. Solutions of Basic Equations

From the five basic eqns. we find that there exist groups of fluid motions and magnetic field as follows

$$\begin{array}{ccccccc} U_n^m & \rightleftarrows & Y_{n+1}^m & \rightleftarrows & U_{n+1}^m & \rightleftarrows & \cdots \\ \downarrow\uparrow & & \downarrow\uparrow & & \downarrow\uparrow & & \\ T_n^m & \rightleftarrows & S_{n+1}^m & \rightleftarrows & T_{n+1}^m & \rightleftarrows & \cdots \end{array} \tag{A.28}$$

$$\begin{array}{ccccccc} V_n^m & \rightleftarrows & U_{n+1}^m & \rightleftarrows & Y_{n+2}^m & \rightleftarrows & \cdots \\ \downarrow\uparrow & & \downarrow\uparrow & & \downarrow\uparrow & & \\ S_n^m & \rightleftarrows & T_{n+1}^m & \rightleftarrows & S_{n+2}^m & \rightleftarrows & \cdots \end{array} \tag{A.29}$$

As in [1], we shall examine the first type motions taking only the first four terms in consideration.

There is no second type motion because the continuity of the magnetic field can not be satisfied on boundary surface.

We expand five scalars $\frac{U_n^m}{r}$, $\frac{V_n^{m+1}}{r^2}$, $\frac{T_n^m}{r^2}$, $\frac{S_{n+1}^m}{r}$ and Θ_n^m by the spherical Bessel functions $J_{n+1/2}\left(\frac{a_j r}{r}\right)$ where a_j's is the roots of $J_{n+1/2}(a_j)=0$. With above expansions the boundary conditions are satisfied.

If all quantities vary as $e^{\lambda t}$, substituting the five scalars, expanded by the spherical Bessel functions, in the basic eqns., we get the eqn. (1).

6. Acknowledgments

The author wishes to express his thanks to Prof. S. Chandrasekhar for his discussion of my previous papers and for informing me of Bishop's paper (1958). My thanks are due to the Director M. Hasegawa of Fukui University and Prof. Y. Saito of Osaka city University for their continuous interest and encouragements in the course of this study and to Dr. T. Rikitake of Tokyo University for his valuable discussions and advice on this problem.

References

Backus F.E. (1955) Phil. Mag. **46**, 1310.
Bishop F.E. (1958) Phil. Mag. 8, **3**, 1342.
Bullard E. (1948) M.N.R.A.S. Geophys. Suppl. **5**, 248.
Bullard E. and Gellman H. (1954) Phil. Trans. **247**, 27.
Chandrasekhar S. (1952a) Phil. Mag. 7 **43**, 501.
Chandrasekhar S. (1952b) Phil. Mag. 7, **43**. 1317.
Chandrasekhar S. (1953a) Proc. Roy. Soc. A **216**, 293.
Chandrasekhar S. (1953b) Proc. Roy. Soc. A **217**, 306.
Chandrasekhar S. (1954) Proc. Roy. Soc. A **225**, 173.
Chandrasekhar S. (1956) Proc. Roy. Soc. A **237**, 476.
Chandrasekhar S. (1957) Phil. Mag. 7, **2**. 845.
Fultz D. and Nakagawa Y. (1955) Proc. Roy. Soc. A **231**, 211.
Fultz D, Nakagawa Y. and Frenzen P. (1954) Phys. Rev. **94**, 1471.
Nakagawa Y. (1956) Jour. Phys. Earth **4**, 85.
Nakagawa Y. (1957a) Proc. Roy. Soc. A **240**, 108.
Nakagawa Y. (1957b) Proc. Roy. Soc. A **242**, 81.
Nakagawa Y. and Frenzen P. (1955) Tellus **7**, 1.
Namikawa T. (1957a) J.G.G. **9**, 182.
Namikawa T. (1957b) J.G.G. **9**, 193.
Namikawa T. (1957c) J.G.G. **9**, 203.
Rikitake T. (1959a) Bull. Earthq. Res. Inst. **37**, 245.
Rikitake T. (1959b) Bull. Earthq. Res. Inst. **37**, 405.
Takeuchi H. and Shimazu Y. (1954) Jour. Phys. Earth. **2**, 73.

Magnetic Viscosity of Magnetite*

By Yoshio SHIMIZU

Geophysical Institute, Tokyo University

(Read October 17, 1959; Received April 14, 1960)

Abstract

Magnetic viscosity of ensemble of medium-sized grains of natural magnetites was examined at various temperatures. It was found that magnetic viscosity coefficient S, defined as $I-I_0=S(Q+\log t)$ where I and I_0 are intensity of magnetization at time t and $t=0$, is proportional to external magnetic field, and S is a linear function of temperature, except at temperatures close to the Curie point and $-160°$C, so far as the Rayleigh region of magnetization is concerned. It seems also that S tends to a finite value according as grain size tends to the order of a single domain.

For ensemble of magnetite grains, S in expression of $\Delta I=S(Q+\log t)$ is very small, and the limit of half life time τ for change in thermoremanent magnetization, expressed by $\tau=\exp\frac{I_{tr}}{2S}$ amounts to 10^{120} years.

Further, the half life time for sedimentary rocks, in which directions of grain magnetization are scattered, with reduction factor w, is about 10^{10} years for $w=1/5$. These results may show that remanent magnetization of igneous and sedimentary rocks have been stable against thermal viscosity during a geologically long time.

1. Introduction

It has long been known that some igneous rocks or baked sediments have very stable remanent magnetization, which was fixed in the direction of the earth's field during the process of cooling from above the Curie temperature (Königsberger, 1932; Thellier, 1938; Nagata, 1940). Since this permanent magnetization was discovered, we have expected that the thermoremanent magnetization of rocks may have fossilized the direction of the geomagnetic field at the period of their formation. It has also been expected that sedimentary rocks may have stable residual magnetization which is due to statistical alignment of the ferromagnetic mineral grains to the ambient magnetic field during sedimentation (McNish and Johnson, 1938; Nagata, Rikitake and Akasi 1943). The studies on palaeomagnetism, which accomplished a remarkable development in recent years, have founded on the above premises.

As for stability of remanent magnetization of rocks, for example, Graham measured the direction of remanent magnetization of many specimens of old sediments cut from folded beds and concluded that those rocks must have maintained the direction of

* Contribution from Division of Geomagnetism and Planetary Physics, Geophysical Institute, Tokyo University, Series II, No. 98

the magnetic field before folding (1949). On the other hand, Kawai observed in certain sedimentary rocks that remanent magnetizations of such rocks are always shifting their directions towards the ambient magnetic field when the rocks were replaced from one direction to another in laboratory (1953). More recently occurrences of such unstable remanent magnetizations have been reported (Creer 1957; Akimoto and Kushiro, 1960). Prior to these, Thellier indicated that the intensity of the isothermal remanent magnetization of some clay decreases proportionally to the logarithm of time for the time intervals from 20 sec to 5×10^6sec. (1938). Such change of magnetization with time has long been known as "magnetic viscosity" or "magnetic after-effect" in the case of metallic ferromagnetics, (Ewing, 1885; Rayleigh, 1887).

It is intended, in the present study, to make investigation of magnetic viscosity of magnetite as the most common ferromagnetic minerals in rocks, by considering its relevance to palaeomagnetism. Measurements were made for various magnetic properties, i.e. susceptibilities, coercive force, magnetic viscosity and thermoremanent magnetization and their thermal variations within the wide range (90°～850°K) of temperatures. The results of the measurements will be given in § 4 and in the last section possible mechanism of the observed magnetic viscosity of remanent magnetization will be discussed.

2. Specimens

Specimens used in the present investigations were natural magnetite grains of iron ore from Kamaishi Mine, Japan. It was confirmed by microscopic examination that each grain *in situ* was composed of crystallites. The chemical composition, lattice parameter, and intrinsic magnetization of the specimens are summarized in Table I.

Table I. Chemical composition, lattice parameter and spontaneous magnetizatoin of specimens.

		weight per cent	mol per cent
Chemical composition	FeO	28.91	47.53
	Fe_2O_3	70.96	52.47
	TiO_2	<0.1	
Lattice parameter		8.3923±0.0010Å	
Spontaneous magnetization at 20°C		92 emu/gr	

In order to make the range of the grain size in a specimen as narrow as possible, grains were classified by means of sieves (specimen No. 1 and No. 2). Extremely fine grains were obtained by crushing in an agate-mortar (specimen No. 3 and No. 4). Four specimens in Table II were thus obtained.

To avoid change in chemical composition of the specimens during experiments, each specimen was sealed in a quartz tube, 4 mm in diameter and 10 cm long, in vacuum of 10^{-3} mm Hg. The lattice parameter of the specimens was examined by X-ray before and after the heating experiments to make sure that no chemical change occurred.

Table II. Summary of structure sensitive magnetic properties of magnetite grains in the present investigations.

properties / specimen	grain size in micron	differential susceptibilities		coercive force in Oe
		reversible in emu/gr	irreversible in emu/gr	
1	270	0.698	0.091	13
2	100	0.493	0.190	19
3	~2	0.429	0.132	50
4	~1	0.314	0.125	66

viscosity coefficient in emu/gr$\times 10^{-2}$	viscosity field constant in Oe	thermoremanent magnetization in emu/gr
0.85	0.096	5.54
0.66	0.035	3.62
0.60	0.046	6.33
0.49	0.039	—

3. Method and Apparatus

The specimen was mounted in a non-inductively wound and electrically heated tublar oven for heating experiments up to 600°C. In cooling experiments, a Dewar vessel containing either liquid oxygen or "dry ice" moistened with alcohol was used. External magnetic field was applied by means of a water-cooled solenoid which is 30 cm long and 5 cm in diameter. The required stability of the magnetic field was obtained by supplying the current to the solenoid from a 6v. battery.

Measurements of the intensity of magnetization were made by an astatic magnetometer. Arrangements of the apparatus are schematically shown in Fig. 1.

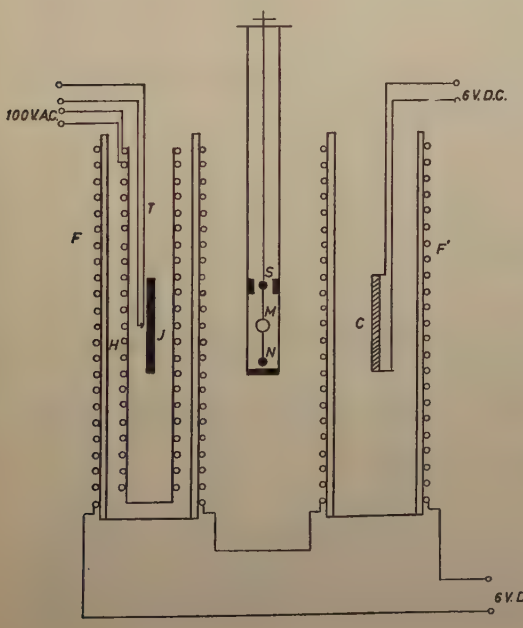

Fig. 1. Schematic view of arrangement of apparatus used for measurements of magnetic susceptibility and viscosity. In the figure, the system SMN denotes an astatic magnetometer, F and F′ are field coils, J is a specimen, C is a compensation coil, and T is a thermo-couple.

Temperature meaurements were made by a calibrated thermo-couple having one junction placed near the mid-point of the specimen. It was proved that the temperature of the specimen could be maintained for several hours at any constant temperature between 15°C and 400°C within 2°C in accuracy and a little worse at higher temperatures; with solid carbon dioxide in the Dewar vessel the temperature was $-77°C \pm 1°C$ for several hours, and when liquid oxygen was used the temperature was maintained at $-183°C \pm 1°C$ for the same length of time. For the purpose of giving intermediate temperatures between $-77°C$ and $-183°C$, the method illustrated in Fig. 2 was used. By this method, however, it was difficult to maintain the constant temperature for more than several minutes.

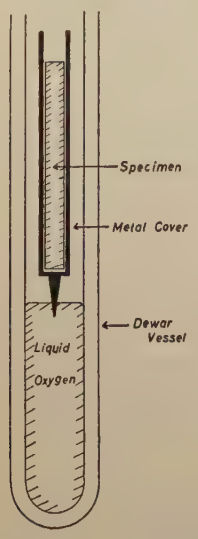

Fig. 2. Schematic figure of apparatus for temperature control between 90°K and 196°K.

For measurements of magnetic viscosity for a point on the virgin curve of magnetization, the following procedure was adopted. The specimen was carefully demagnetized thermally in a non-magnetic space and was brought into the apparatus, in which the vertical component of the terrestrial magnetic field was kept compensated by appropriate current of the field solenoid. Then the whole apparatus was allowed to reach thermal equilibrium. The deflection of the magnetometer corresponding to instantaneous magnetization due to the application of the external field, was compensated by appropriate currents through the carlibration coil, since we are interested only in the subsequent small variation of magneti zation with time. During the measurements, no change of the currents in the field coil and in the calibration coil was detected.

The measurements of the total, reversible and irreversible differential susceptibilities were made, by observing small changes in magnetization caused by slight changes in applied field. The definitions of these quantities are

$$K_{tot}=\frac{\Delta I}{\Delta H_0}, \qquad (1)$$

$$K_{rev}=\frac{1}{2}\left(\frac{\Delta I_1}{\Delta H_1}+\frac{\Delta I_2}{\Delta H_2}\right), \qquad (2)$$

$$K_{irr}=K_{tot}-K_{rev}, \qquad (3)$$

where ΔI, ΔI_1, ΔI_2; ΔH_0, ΔH_1 and ΔH_2 are shown in Fig. 3. In the present study, we took the value of ΔHs ($s=0$, 1 and 2) as 0.25 Oe.

Measurements of coercive force were made by another apparatus using the ballistic method, description of which is given elsewhere (Uyeda, 1958).

4. Results

A typical set of measurements is shown in Fig. 4. It illustrates (ΔI, log$t$) relation at various temperaturs, where ΔI is the amount of change in magnetization during the time t, t being measured from the moment of the application of the external field, H. The

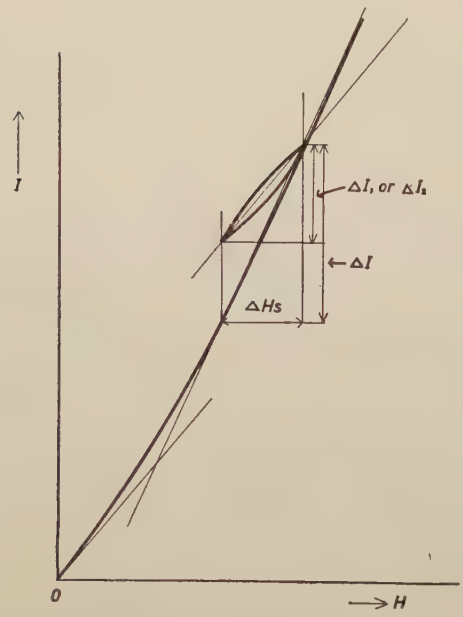

Fgi. 3. Illustration of measurement of reversible and irreversible differential susceptibilities, where ΔHs denotes a small variation of magnetic field. (s=0, 1 and 2).

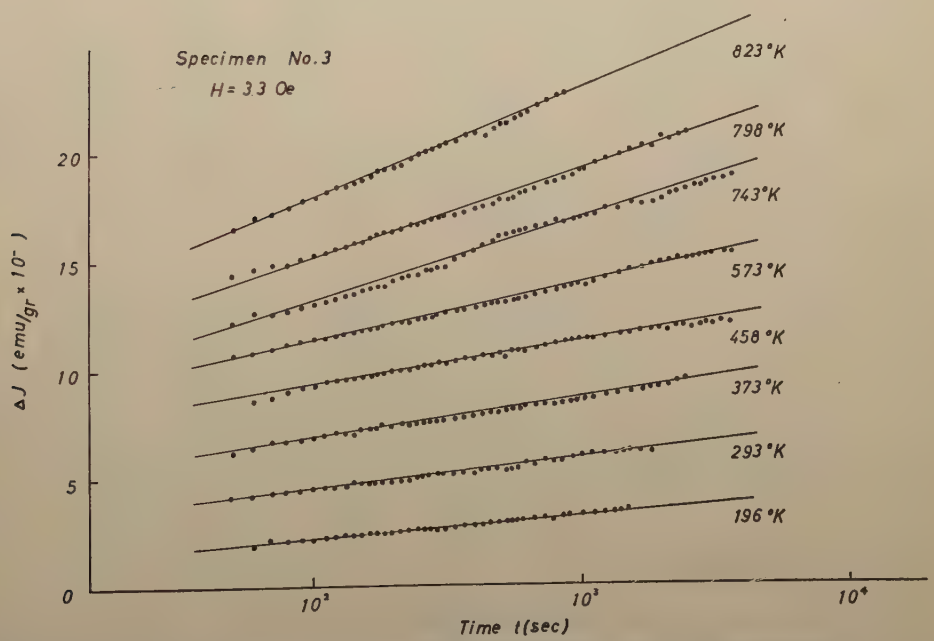

Fig. 4. Variation of magnetization as a logarithmic function of time t after a sudden increase in applied magnetic field. The temperature at which the experiments were made are indicated under the curves.

Note: The zero of the scale of ordinates is arbitrary and the relative position of the graphs have been chosen for convenience in drawing.

applied magnetic field H in the present experiments is 3.3 Oe. The result shows that apparent time variation of magnetization of magnetite grains, ΔI, is proportional to $\log t$ within the time intervals from 30 to 2,000 seconds, that is,

$$\Delta I = \text{const.} + S \log t, \qquad (4)$$

where the slope, S, is called the magnetic viscosity coefficient. If the applied field H (=3.3Oe) is suppressed after an instant application, the residual magnetization ΔI_r decreases gradually. (ΔI_r, $\log t$) curve shown in Fig. 5 represents ΔI_r as a linearly decreasing function of $\log t$, the slope of which is about half of that of the above-mentioned experiment; i.e. S of the former is 0.45×10^{-2} emu/gr and that of the latter is 0.85×10^{-2} emu/gr for the specimen No. 1.

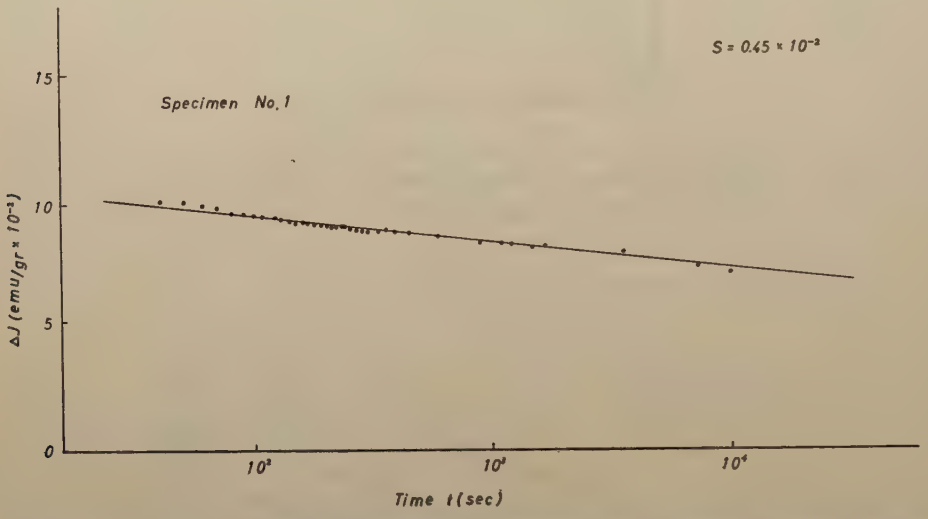

Fig. 5. Variation of remanent magnetization as a logarithmic function of time t after a suppression in applied magnetic field.

Fig. 6 illustrates the field dependence of the magnetic viscosity coefficient S on the virgin curve of magnetization of specimen No. 2. The figure shows that S is proportional to the applied magnetic field H, provided that the field is less than the coercive force H_c of the specimen. The magnetic viscosity coefficient S has been known, for case of metallic ferromagnetic material, to become maximum when the intensity of the applied field approaches that of coercive force (Street and Woolley, 1949). Our experiments, however, did not cover such a wide range of external field because of the limitation of the apparatus.

The fifth and sixth columns of Table II and Fig. 7 represent the relation between the viscosity coefficient S and coercive force H_c at the room temperature. The abscissa of Fig. 7 is represented by reciprocal of H_c. Our experiment shows that the magnetic viscosity coefficient S decreases as the grain size decreases and hence the coercive force increases.

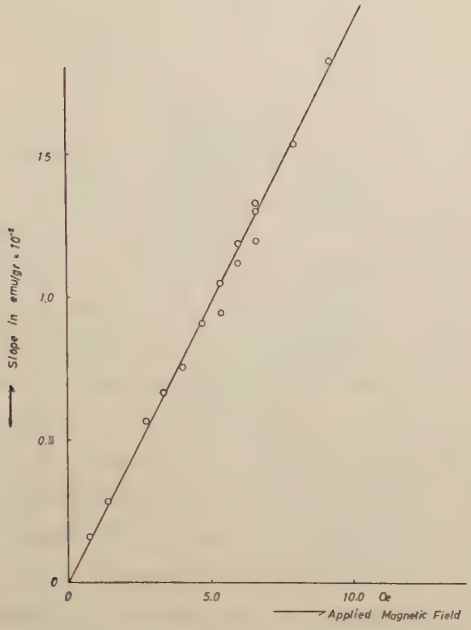

Fig. 6. Variation of magnetic viscosity coefficient S as a function of the applied magnetic field intensity.

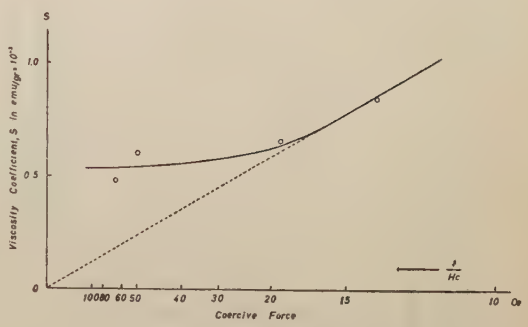

Fig. 7. Variation of magnetic viscosity coefficient S as a function of reciprocal value of coercive force.

Fig. 8 illustrates the temperature dependence of the magnetic viscosity coefficient S as deduced from the experiments shown in Fig. 4. The applied field is 3.3 Oe throughout all three experiments. Measurements near the temperatures of liquid oxygen were done only for the specimen No. 1. At the temperatures near the Curie point and near $-160°C$, the experimets required extremly highly accurate temperature control. Even under a good control of temperature, the duration of observation had to be shortened to only several minutes. In these figures, the most remarkable characteristics are

(i) There are two high peaks of S at temperatures near the Curie point and near the transition point at $-160°C$. These peaks will be refered to as S_C and S_L in the following.

(ii) Between the two peaks S_L and S_C within a fairly wide range of temperature, S varies as a linear function of absolute temperature T.

(iii) The height and the temperature of the peak S_C depend on the grain size of the specimen, and hence on the coercive force.

In order to determine the temperature tendency of viscosity field constant $S_v = S : X_{irr}$, which has been introduced in the Néel's theory given below (1950, 1955), the temperature variations of reversible and irreversible differential susceptibilities are measured between 196°K and 850°K. An example of the results is shown in Fig. 9.

Fig. 10 (a), (b) and (c) show the thermal dependence of S_v as deduced from the experiments in Fig. 8 and 9, together with the temperature dependence of the coercive force. The figures indicate that S_v varies linearly within only the limited range of temperatures from 200°K to 400°K or more, and at about 600°K it reaches the broad maximum, and then shows a minimum. Above this minimum, the $S_v - T$ curve has a sharp

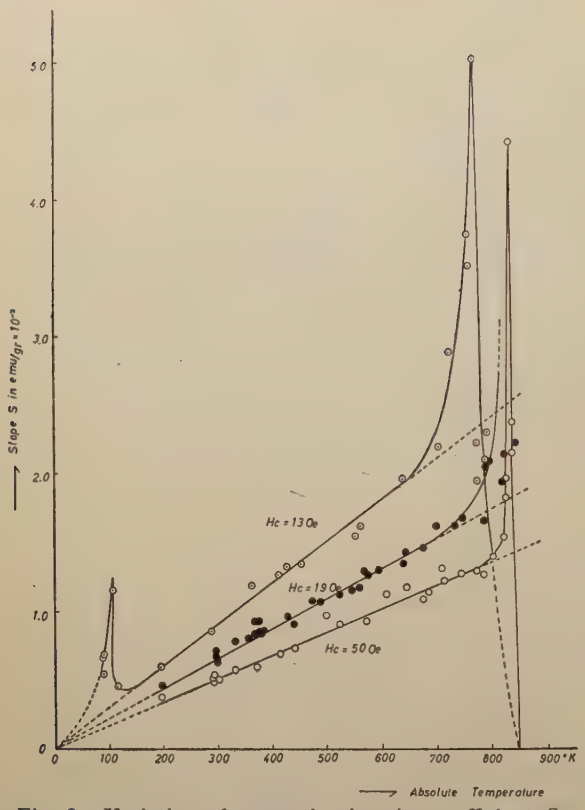

Fig. 8. Variation of magnetic viscosity coefficient S as a function of absolute temperature. Coercive force of each specimen is indicated on the curves.

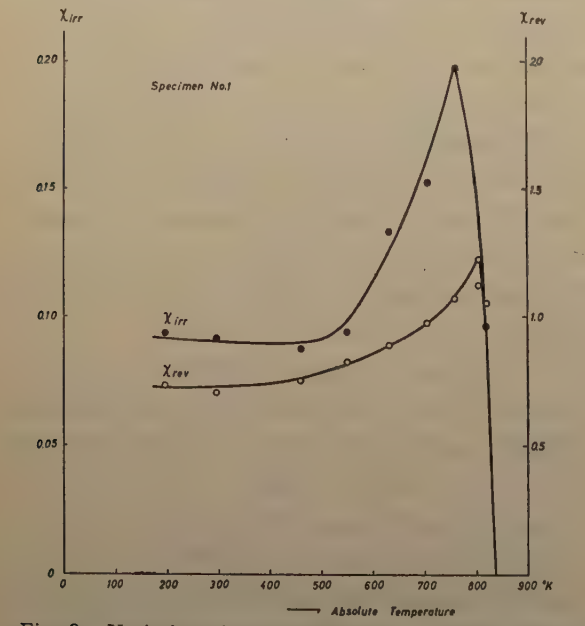

Fig. 9. Variation of reversible and irreversible differential susceptibilities as a function of absolute temperature.

apex near the Curie point. Similarly as in Fig. 8, the higher the coercive force of specimen is, the nearer is the apex to the Curie point. Such behavours of S_v will be discussed in next section.

In Fig. 11 are plotted the values of total, reversible and irreversible differential susceptibilities against the intensities of the applied magnetic field. The figure shows that the reversible susceptibility is independent of the field H, and the irreversible one is proportional to H. Hence, the instantaneous magnetization after the application of the magnetic field H may be expressed empirically as follows

$$I=AH+BH^2, \qquad (5)$$

where A denotes the reversible susceptibility and $2BH$ is equivalent to irreversible differential susceptibility. Eq. (5) expresses essentially the Rayleigh's first law of magnetization in a weak field.

5. Discussions

A theory of magnetic viscosity has been proposed by Néel by assuming that, in a certain region of magnetization, the Bloch wall may cross over obstacles by thermal activations (1950, 1951 and 1955). According to the Néel's theory, the effect of thermal agitations can be replaced by a fluctuating viscosity field $H_f(t)$ in addition to the applied field H. $H_f(t)$ being

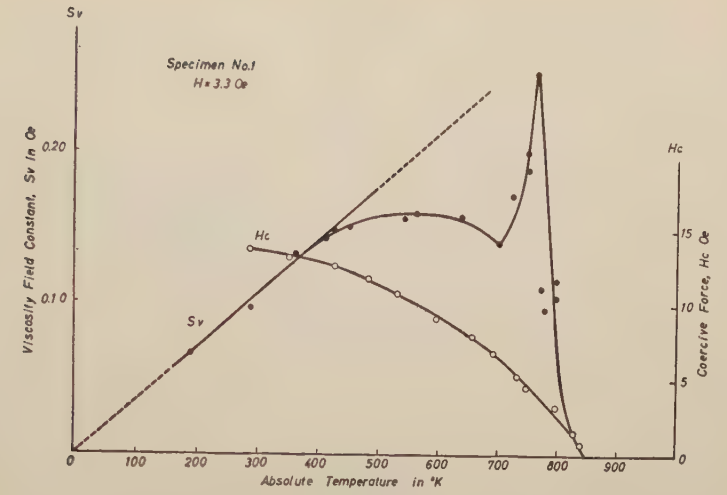

(a)

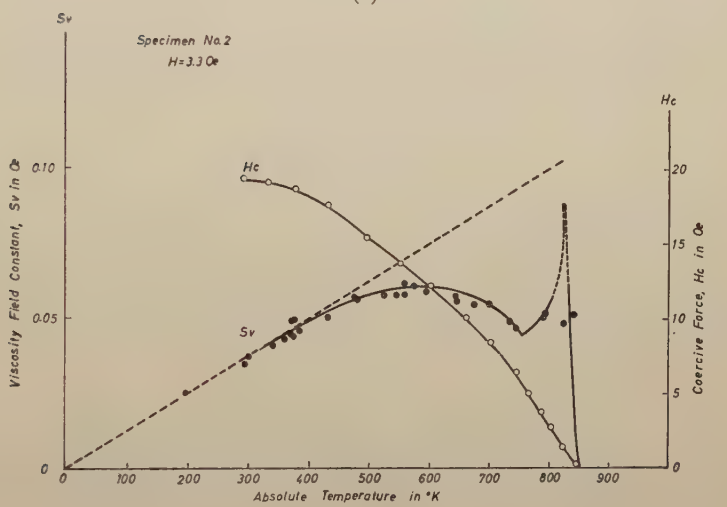

(b)

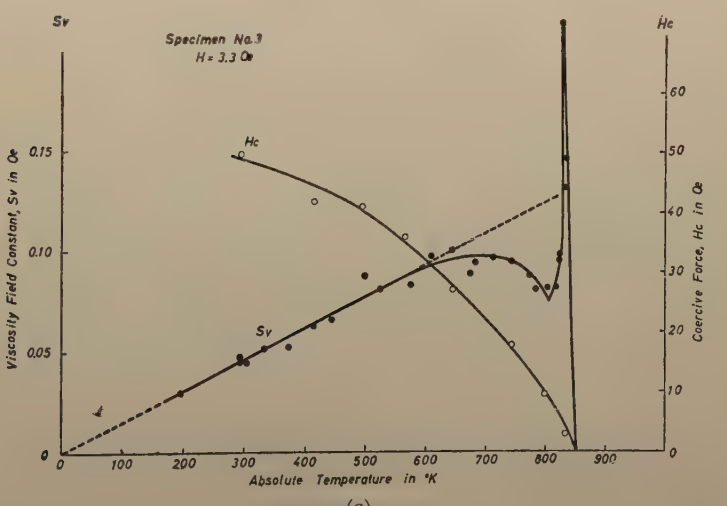

(c)

Fig. 10. (a), (b) and (c) Variation of magnetic viscosity field constant S_v as a function of absolute temperature, together with variation of coercive force with temperature.

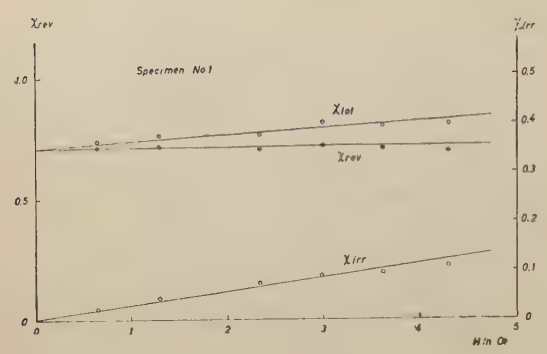

Fig. 11. Variation of total, reversible and irreversible differential susceptibilities as a function of applied magnetic field.

given by

$$H_f(t)=S_v(Q+\log t)\,, \qquad (6)$$

where Q is a numerical constant of the order of 40 or 50, t the time interval since the beginning of the application of the field H, and S_v, which has dimension of magnetic field, is a characteristic constant of the specimen, depending on temperature. Thus, intensity of magnetization I after a time t has been derived by Néel as

$$I=I_0+\chi_{irr}S_v(Q+\log t)\,, \qquad (7)$$

where I_0 is magnetization in case of absence of the viscosity field and χ_{irr} the irreversible differential susceptibility.

In the case of Rayleigh region, the instant magnetization I_0 is equal to $AH+BH^2$ and the irreversible susceptibility χ_{irr} is equal to $2BH$ as can be seen in § 4. Thus, eq. (7) can be expressed as

$$I=AH+BH^2+2BHS_v(Q+\log t)\,. \qquad (8)$$

After suppression of the applied field H, the remanent magnetization is given by $\frac{1}{2}BH^2$ and the irreversible susceptibility by $-BH$, so that the remanent magnetization I_r at the time t after the suppression of the field becomes

$$I_r=\frac{1}{2}BH^2-BHS_v(\log t-\log t')\,, \qquad (9)$$

where t' denotes the time interval to keep applied field as H. These expressions were verified in the present experiments, as shown in Fig. 4 to Fig. 6, namely, the viscosity coefficient S of $\log t$, which is equal to $2BHS_v$ in eq. (8), is proportional to H, and S of the remanent magnetization, which is equal to BHS_v, is about a half of that of the former. Numerical values of χ_{irr} and S_v for present magnetite are summarized in Table II, where χ_{irr} is about 0.1 emu/gr, and S_v is about 0.05 Oe at the room temperature.

It may be also expected in the Bloch wall displacement theory of magnetic viscosity that the magnitude of S for the same substance decreases according as the height of barrier increases with increase in coercive force, and S should become zero when the height of barrier becomes infinitely large. According to our experimental results shown in Fig. 7, however, it seems likely that S tends towards a certain finite value, when coercive force tends to infinity. This could be interpreted as that coercive force increases

with decrease in grain size but the former tends to a limit value for a single domain value as its extremum condition.

Now, quantity S_v, which is introduced in eq. (6) is significant in relation to mechanism of magnetic viscosity. According to the Néel's interpretation, the Bloch wall may cross obstacles by help of the internal dispersion field which is derived from small oscillations of each spontaneous magnetization around the mean direction of domain magnetization (1950, 1951 and 1955). Based on the above-mentioned model, it is given that

$$S_v = \sqrt{\frac{4\pi kT}{3v}} Q^{-1/2}, \qquad (10)$$

where k is Boltzmann constant, T absolute temperature, and v is volume of Barkhausen discontinuity.

On the other hand, another theory has been proposed by Street and Woolley (1949, 1950, 1952 and 1955). In their theory, the thermal agitations are supposed to affect heights of the barriers which opposed the wall movements. Using the theory of rate process, the following relation was derived, i.e.,

$$S_v = \frac{kT}{2vI_s}, \qquad (11)$$

where I_s is spontaneous magnetization and v is volume of the Barkhausen domain. The Néel's theory on magnetic viscosity for single domain grains is essentially similar to the Street and Woolley's (Néel; 1949 and 1955).

As can be seen in eq. (10) and eq. (11), the thermal variation of S_v is given differently in the two theories; if v is independent of T, S_v varies proportionally to $T^{1/2}$ in eq. (10), but to T in eq. (11).

In the results of the present experiments, however, S_v showed some complicated features, as can be seen in Fig. 10 (a), (b) and (c). However, by refering to the above-mentioned two theories, the present results may be interpreted for three temperature ranges as in the followings.

(i) ca 200°K$<T<$ca 400°K. In this range of temperature, S_v is proportional to T. According to the theories summarized above, the viscosity field in this range is not likely to be controlled by the internal dispersion field, but by the fluctuation of the heights of barriers.

(ii) ca 400°K$<T<$ca 700°K. S_v increases slowly, deviating from the linearity of S_v–T relation, and reaches maximum and then decreases with increase in temperature. On the other hand, $S=\chi_{irr}\cdot S_v$ is about a linear increase function of T, as can be seen in Fig. 9, whereas χ_{irr} augments gradually with temperature. Hence, the increase of S_v with temperature becomes slow and deviates from the linear relation between S_v and T.

(iii) ca 700°K$<T$. At temperatures very close to the Curie point, with increase in temperature S_v increases again rapidly, forms a very sharp apex and then tends to zero rapidly. The temperature at the apex of S_v coincides with that of S and also that of the maximum of χ_{irr}. This sharp inarease of S_v may prove that the thermal increase

of S is now more rapid than that of χ_{irr}. Further, the temperature of the apex is different from specimen to specimen, being dependent on grain size. It is also concluded that coercive force of the specimen becomes, at this temperature range, as small as the order of magnitude of external magnetic field. This result might be interpreted as follows. At the temperatures very close to the Curie point, crystal anisotropy of specimen becomes very small and thickness of Bloch wall becomes larger and larger until the meaning of domain conception is lost, whereas the shape anisotropy does not decrease so rapidly compared with the crystal anisotropy, because the shape anisotropy energy is proportional to I^2 and crystal energy, according to Zener-Carr's theory, is proportional to the higher power than I^2 (Zener, 1954: Carr, 1958). In such a state, each grain may be regarded as a single domain grain which has a critical field $H_c=K/I_s$ for rotation of spontaneous magnetization, where K denotes shape energy. Magnetic viscosity of such single domains may be treated by the Néel's theory for single domain grains. That is to say, provided that intensity of magnetic field H is close to critical field H_c of grains, S and S_v are approximately given by

$$S=\frac{2kT}{v_{max}(H_{cm}-H)}, \tag{12}$$

$$S_v=\frac{2H_{cm}kT}{v_{max}I_s(H_{cm}-H)}, \tag{13}$$

where H_{cm} denotes maximum critical field, and v_{max} is maximum volume of single domain grains. If H_{cm} approaches to H with increase in temperature, factor $(H_{cm}-H)$ or $H_{cm}/(H_{cm}-H)$ in eq. (12) or eq. (13) becomes rapidly large.

The present results are compared with those of metals and alloys made by Courvoisier (for steel; 1954), Barbier (for alnico; 1953), Street, Woolley and their colleagues (for alnico and other several alloys; 1949, 1951 and 1955), and Pescetti and Barbier (for alloy of Cu, Ni and Be; 1956). Generally speaking, the present results are in qualitative agreement with those for metallic ferromagnetics, though the apex of S_v at a temperature near the Curie point is not found in their results.

6. Stability of Remanent Magnetization

Viewed from the results obtained in the present study, stability of remanent magnetizations obtained by various procedures of magnetization such as thermoremanent magnetization (TRM) and detrital magnetization (DRM), etc. will be discussed. In ferromagnetic specimen having such permanent magnetization, the Bloch wall has been trapped by an obstacle at a position different from that corresponding to zero magnetization. Under the constant temperature and constant pressure, distribution of such obstacles, which are due to imperfection of crystal such as fluctuations of internal stress, impurities, or shape anisotropy etc., is expected to be kept constant in the interior of the crystal, provided that there is no secondary chemical alteration. Under the effect of thermal agitations, the Bloch wall may cross over trapping obstacle. Even if this probability is negligibly small in the laboratory time scale, its effect should become

appreciably large for very long time such as geological time scale. For the laboratory time scale, it is proved that the relation $\Delta I \propto \log t$ holds for natural magnetites also. However, it may be clear, on the other hand, that the total amount of change in intensity of remanent magnetization caused by magnetic viscosity should tend to a finite value when t becomes infinite. Therefore, amount of decay of remanent magnetization estimated by means of the law $\Delta I \propto \log t$ during a certain time interval should be uppermost limit, and consequently the decay time for a certain amount of change in I_r calculated by the formula should be its lowest limit. By considering the above-mentioned condition, stability of remanent magnetization for geologically long time could be estimated as in the following.

When the direction of the external magnetic field is antiparallel to that of thermoremanent magnetization of a rock specimen, change in magnetization $I(t)$ during t is given by

$$I(t)=I_{tr}-S(\log t-\log t'), \qquad (14)$$

where I_{tr} is the initial thermoremanent magnetization and t' is the time intervals when the magnetic field kept parallel to the direction of thermoremanent magnetization at room temperature. If t' is negligibly small compared with t, the "half-life" time of thermoremanent magnetization will be given by

$$\log t=\frac{I_{tr}}{2S}. \qquad (15)$$

Numerical estimation based upon actual values given by figures in Table II, results in that the "half-life" time of the thermoremanent magnetization of ensemble of magnetite grains is in order of 10^{120} years, which is much larger than the age of the earth. Thus, it may be concluded that thermoremanent magnetization of igneous rocks is extremely stable against thermal viscosity. In other words, thermoremanent magnetization of igneous rocks ought to have well reserved its initial condition during their whole life, provided that there has been no appreciable chemical modification.

In the case of detrital remanent magnetization of sedimentary rocks, which is considered to be due to statistical alignment of magnetite along the earth's magnetic field whose remanent magnetization is originally due to thermoremanent or chemical remanent magnetization (Kobayashi, 1956). The "half-life" time may be given as

$$\frac{wI_{tr}}{2}=S\log t, \qquad (16)$$

where w denotes an efficienency of the alignment.

Eq. (16) gives, for example, that $t\simeq 10^{35}$ years for $w=1/3$ and $t\simeq 3\times 10^5$ years for $w=1/10$. According to the results of evaluation of w of some actual sediments, its magnitude is between $\frac{1}{10}$ and $\frac{1}{3}$ (Nagata, 1953). In such a case, stability of the detrital remanent magnetization against thermal viscosity is fairly high.

On the bases of above mentioned estimations, we can place some reliance upon the results of palaeomagnetic studies by means of igneous or sedimentary rocks, provided

that due cautions are taken in selecting the rocks.

Acknowledgment

The author wishes to record his indebtedness to Professor T. Nagata for his constant instruction and encouragement during this work and to Drs, S. Akimoto and S. Uyeda for their kind criticisms and suggestions. His thanks are also due to Dr. T. Katsura (Tokyo Institute of Technology) for his chemical analysis of the specimens.

References

Akimoto S. and Kushiro I (1960) J. Geomag. Geoelect. **11**, 94.
Barbier J.C. (1953) Théses Grenoble.
Carr W.J.Jr. (1958) J. Appl. Phys. **29**, 436.
Courvoisier P. (1945) Sitz der Bayer. Ak. Wiss. **250**, 89.
Creer K.M. (1957) Phil. Trans. Roy. Soc. Lond. **250**, 130.
Ewing J.A. (1885) Phil. Trans. Roy. Soc. Lond. **176**, 554.
Graham J.W. (1949) J. Geophys. Res. **54**, 131.
Kawai N. and Kume S. (1953) J. Geomag. Geoelect. **5**, 66.
Kobayashi K. (1959) J. Geomag. Geoelect. **10**, 99.
Königsberger J.G. (1932) Beitr. Angew. Geophys. **4**, 385.
McNish A.G. and Johnson E.A. (1938) Terr. Mag. **43**, 393.
Nagata T. (1940) Bull. Earthq. Res. Inst. **18**, 281.
Nagata T. (1953) Rockmagnetism (Tokyo, Maruzen).
Nagata T., Rikitake T. and Akasi K. (1943) Bull. Earthq. Res. Inst. **21**, 275.
Néel L. (1949) Ann. de Geophys., **5**, 99.
Néel L. (1950) J. Phys. Rad. **11**, 49.
Néel L. (1951) J. Phys. Rad. **12**, 339.
Néel L. (1955) Advance in Phys. **4**, 191.
Pescetti D. and Barbier J.C. (1956) C.R. Acad. Sci. Paris **243**, 1740.
Phillips J.H., Woolley J.C. and Street R. (1955) Proc. Phys. Soc. **B68**, 845.
Rayleigh Lord (1887) Phil. Mag. **23**, 225.
Street R. and Woolley J.C. (1946a) Proc. Phys. Soc. **A62**, 562.
Street R. and Woolley J.C. (1946b) Proc. Phys. Soc. **A63**, 509.
Street R., Woolley J.C. and Smith P.B. (1952) Proc. Phys. Soc. **B65**, 679.
Thellier E. (1938) Ann. Inst. Phys. Globe **16**, 157.
Uyeda S. (1958) Japan Journ. Geophy. **2**, 1.
Zener C. (1946) Phys. Rev. **69**, 1335.

The Structure of the Atmospheric Electric Field

By Toshio OGAWA

Geophysical Institute, Kyoto University

(Read December 7, 1959; Received March 26, 1960)

Abstract

Simultaneous records of the atmospheric electric potential gradient at three stations which make a regular triangle with sides of about two km, were compared with each other during the period of January 8–13, 1956, including a cloudy day as well as fine days. Expanding the daily course of the potential gradient on each day and at each station into Fourier series of 12 terms, the spectral distribution of the square of the amplitude of each component was obtained and the spectrum of the field was given by n^{-4} in an undisturbed day, n expressing the harmonic term. On theoretical grounds, assuming the distribution of space charge concentration characterized by its scale and its density within the lower layer of the atmosphere, the spectral distribution of field energy was suggested to be represented by n^{-7} in the intermediate range of n. The result was proved to be consistent with the above analytical result. The factor causing the disturbance in the spectrum was looked for into the atmosphere using the aerological data. It was found that the turbulent situation of the air in the lower altitudes up to three km would control the structure of the atmospheric electric field.

1. Introduction

Horizontal distribution and time variation of the atmospheric electric potential gradient have been investigated in a series of surface measurements carried out in Kyoto since 1955. The purpose of this paper is to find out the structure of the atmospheric electric field in electrically undisturbed day and the cause of the perturbation in the field.

On land areas of the earth, especially less removed from sources of pollution, the atmospheric electric field which is usually measured within the turbulent and contaminated exchange layer is subject to great local variations, which mask almost entirely the universal variation of the field. Even in a so called undisturbed day there are so many kinds of variations, regular and irregular, in the field at the earth's surface that it is impossible to attribute each variation to a corresponding origin. To see the general feature of the field, the statistical analysis of large amount of data is usually required, which offered much of the existing information, leaving the choice of periods for the analysis to the investigator. In the statistical procedure of analysis, irregular variations are eliminated and only regular variations are emphasized, and the characterizing and pronouncing daily curve of change with local time is obtained, which is regarded as the representative of the atmospheric electric field. However, it is not

enough to conclude the representativeness of the variation curve of the field thus obtained to that in fair weather. Can it be acceptable that the eliminated irregular variations with periods smaller than diurnal and semi-diurnal are not significant in the atmospheric electric field profile? Such irregular variations must be related with the turbulence in the atmosphere, and they are the substantial components which the field consists of.

As has been pointed out by Kasemir (1950), atmospheric electric processes such as changes in the potential gradient and space charge density are related with the relaxation time of the air. So far as treating variations with rather larger periods than the relaxation time, the atmosphere is considered to be in a state of quasistatic equilibrium and the principle of the quasistatic state can be adopted. Since actual values of the atmospheric relaxation time are from 5 to 40 minutes at the earth's surface, it is possible to apply the quasistatic principle to variations with periods of over one hour.

In this state the vertical current density i is considered to be constant with altitude, and the space charge density ρ which is arised from the conductivity change with altitude is given by

$$\rho=\varepsilon i\frac{d}{dz}\left(\frac{1}{\lambda}\right), \tag{1}$$

where ε is the atmospheric permittivity and λ is the conductivity. As the conductivity of the atmosphere increases almost exponentially with height, the space charge density is considered to decrease with height in the same manner. In actual, smaller conductivities due to the condensation nuclei concentration produce the positive space charge in the lowest altitude of the atmosphere.

The intricate variations in the atmospheric electric field at the earth's surface are, in fair weather, considered to be caused by changes of the space charge configuration, which is, of course, influenced by the atmospheric turbulence. It is also the purpose of this paper to learn how the atmospheric electric field is modified by the day-to-day variation in the intensity of the turbulence in the lower atmosphere.

2. Experimental and Analytical Results

The circumstance of the measurement for the atmospheric electricity is as follows. Measurements were made at three points which make a regular triangle with sides of about two km in the north-east district in Kyoto city which has the population of about one million and no big industrial area. The reason why the three points were used is to find out the chance that very local changes in specified points might disturb the generality of the results. The surface stations were all located atop the buildings nearly 10–15 m high to avoid the disturbances near the ground. Throughout the year and especially in the cold season, it is excelled in westerly wind over Kyoto.

The reproduction of the records for the period of January 8–13, 1956, is presented in Fig. 1, the values of the potential gradient being normalized to the mean value for each day and each station. According to the report of Kyoto Meteorological Observa-

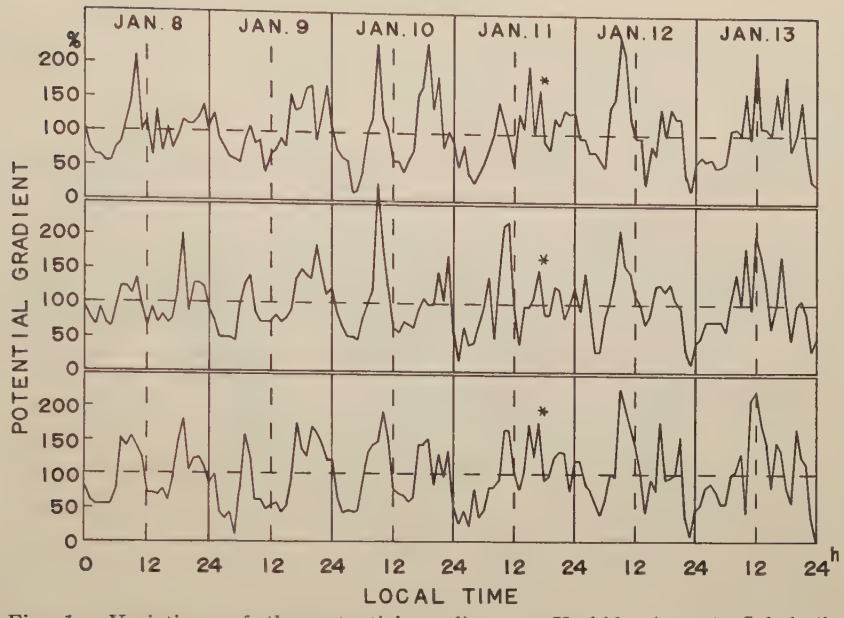

Fig. 1. Variations of the potential gradient at Yoshida (upper), Sokokuji (middle) and Shimogamo (lower) on January 8–13, 1956. The value of the potential gradient is normalized to its mean value for each day and each station.

Table 1. Meteorological conditions during the period of January 8–13, 1956

Meteorological conditions \ Date	Jan. 8	Jan. 9	Jan. 10	Jan. 11	Jan. 12	Jan. 13
Cloudiness, average, 0–10	2.0	1.0	1.8	0.0	0.8	5.3
Wind speed, average (m/s)	2.1	2.0	1.4	1.4	0.9	0.3
Sunlit time (hour)	6.9	8.8	8.2	5.1	7.6	0.7

tory, since January 8, Japan Islands were in the typical winter type distribution of atmospheric pressure, high in the west and low in the east. The surface meteorological conditions—cloudiness, wind speed and sunlit time—on each day are given in Table 1. During this period there was no precipitation except January 11 when a minor shower cloud with the precipitation 0.0 mm swept over the stations at about 17 o'clock. The effect of the minor shower was quite insignificant as shown with stars in the figure. At no time during this period was a negative value of the electric field observed. Nor did any other changes in the field occur which could be attributed to visible meteorological effects. The remarkable feature given in Fig. 1 is that double periodic curves with one maximum in the forenoon and in the afternoon respectively were recorded on January 8, 9, 10 and 12 at all the stations, but on January 11 and 13 single periodic curves with the maximum at about noon were found. A same example was given by

Israël (1955), and it was examined from the synoptical aspect by Dolezalek (1957). In a comparison between three stations the general features with larger periods such as diurnal or semi-diurnal are similar to each other, but there can be seen some different points in detail.

Using the hourly values normalized to the mean value, over a 24 hours period for each day and each station, the variations were expanded into Fourier series of 12 terms and the daily spectral distributions of the square of the amplitude, E_n^2, of each component were obtained. The result of this procedure, which is rather divergent, is shown with logarithmic scales in Fig. 2 but it can be seen that there is to some degree the regularity in the spectra. In general, there is a peak at the second term in the spectral distribution and the values of E_n^2 decrease when terms become higher, and in the range higher than 6th or 7th term the spectral distribution is subject to a great fluctuation. In the intermediate range from 2nd term to 6th or 7th term, however, rather fixed value of characteristic slope is seen on January 10, 12 and 9. The most typical example (January 10) gives the spectral distribution of n^{-4}. On the other hand the estimation of the value of the power is not possible on January 8, 11 and 13. The question arises as to what value of the power to be in an undisturbed condition,or what is responsible for the disturbance of the spectrum. A theoretical consideration will suggest in the next section that -4 is available to the value of the power of the spectrum with an appropriate model of the field structure when there is not any disturbance. The preceding experimental value on January 10 is in agreement with this value.

The factor which controls the atmospheric electric field profile is the distribution of pollution particles with altitude, which is determined by the intensity of turbulence in the lower atmosphere. Then it will be the turbulent situation in the lower atmosphere that disturbs the spectrum of the field. Air temperature and wind volocity distribution with altitude may be the main determining factors in the turbulence of the air. The air temperature and the wind velocity at Yonago Meteorological Observatory were shown with altitude in Fig. 3. The values at 12 o'clock in the mean local time were used for the elements. Yonago is located about 200 km to the west of Kyoto and the upper air mass trajectory for 850 mb level passing over Kyoto came from over Yonago during the period.

Sagalyn (1958) gave the criterion to see the exchange layer. "The temperature distributions always show an adiabatic temperature gradient throughout the exchange layer with a change to a more stable lapse rate at the top of this region." This criterion suggests that the upper boundary of the exchange layer is 2–3 km above the ground in this period. The space charge constituting the atmospheric electric field can not leak out from the top of this exchange layer and may be distributed within it because of the stable region over the exchange layer. Thus the turbulent situation of the air was examined up to 3 km. To find out the effect of the turbulence of the air on the atmospheric electric field, the author calculated the Richardson number

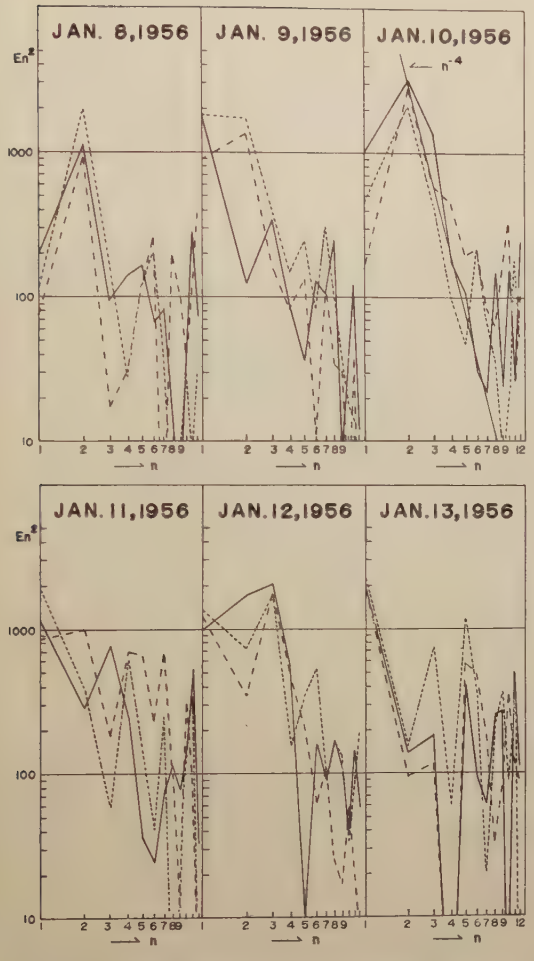

Fig. 2. Daily changes in the spectral distribution of the square of the amplitude expressed in percentage. n is the harmonic term. Full line—Yoshida, dotted line—Sokokuji, and dashed line—Shimogamo.

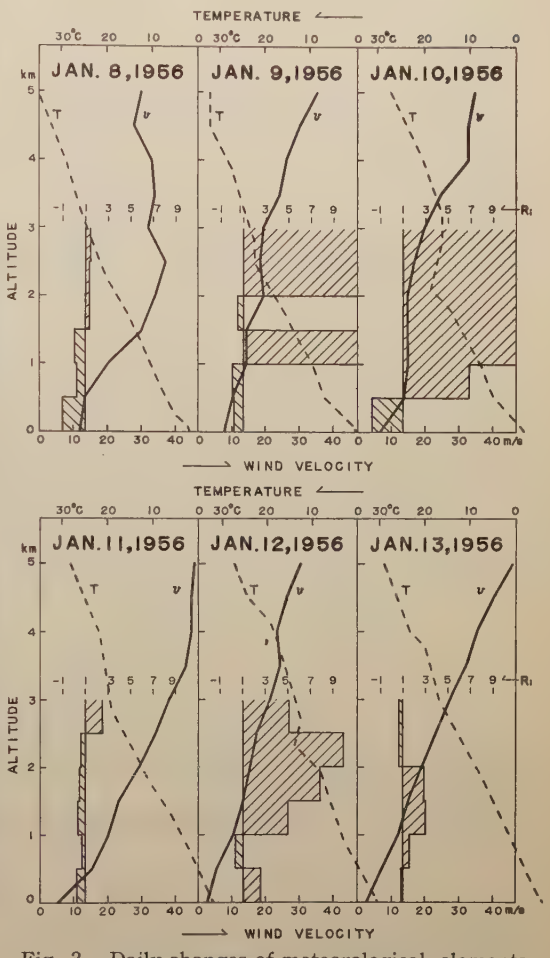

Fig. 3. Daily changes of meteorological elements, air temperature (T) and wind velocity (v), and calculated Richardson number (R_i) with altitude at Yonago.

$$R_i=\frac{g\left(\frac{\partial T}{\partial z}+\Gamma\right)}{T\left(\frac{\partial v}{\partial z}\right)^2}, \qquad (2)$$

which represents a criterion to decide whether turbulence will subside or increase, where T is the absolute temperature, v is the mean velocity, g is the acceleration due to gravity and Γ is the adiabatic lapse rate. This is given in Fig. 3 in which the calculated values are taken in steps every 500 m. From a comparison between Fig. 2 and Fig. 3 it can be seen that there is a correspondency from day to day between the spectrum of E_n^2 and the distribution of R_i with altitude. The thicker the layer of $R_i>1$ in Fig. 3 is, the more systematic the spectral distribution of E_n^2 in Fig. 2 becomes, and the value of the power of the spectrum tends to converge a definite one. Thus

the instability of the air may result in the modification of the spectrum.

3. Theoretical Consideration

As in the previous analysis, the time variation of the atmospheric electric potential gradient at the earth's surface may be expressed in terms of the Fourier series:

$$E=E_0+\sum_n E_n \sin(nt+\alpha_n), \tag{3}$$

that is, it is composed of various simple harmonic components superposed on the mean value.

It is interesting to give one description of the atmospheric electric field by introducing following the two concepts; geometrical scale and electrostatic energy. In the first place, space charge configuration causing variations in the electric field should bec onsidered. Suppose that there are many ranks of space charge concentrations by which the corresponding harmonic terms of the field variation can be caused, and any rank of space charge concentration is in a limited region with a characteristic length Λ (scale) and also electrically characterized by its density ρ. The scale Λ is proportional to the reciprocal of the rank n, i.e.

$$\Lambda \propto \frac{1}{n}. \tag{4}$$

It is assumed that there is no mutual interaction between concentrations both dynamically and electrically, and each of concentrations is located as shown in Fig. 4. It follows that the height of each rank of concentrations, H, is proportional to the scale as

$$H \propto \Lambda. \tag{5}$$

Next, any rank of space charge concentration is assumed to have its own density which is proportional to its scale, i.e.

$$\rho \propto \Lambda. \tag{6}$$

The space charge density of the concentration with a larger scale contributes to the total space charge density distribution with altitude in the higher levels of altitude as well as in the lower levels. On the other hand, the space charge density with a smaller scale contributes in only lower levels; that is, the total space charge density in the lower levels is the result of the contribution from concentrations with larger and smaller scales. These interrelationship between n, Λ, H and ρ is illustrated in Fig. 4 and Table 2. It is acceptable as a first approximation to consider such space charge configuration. In the regions of both larger and smaller values of n, the above mentioned model becomes at variance with the reality and is valid only for the intermediate range of n.

Using the above fundamental relations the atmospheric electric energy spectrum can be led. The total quantity of any rank of space charge concentration characterized by the scale Λ and the density ρ, is expressed by

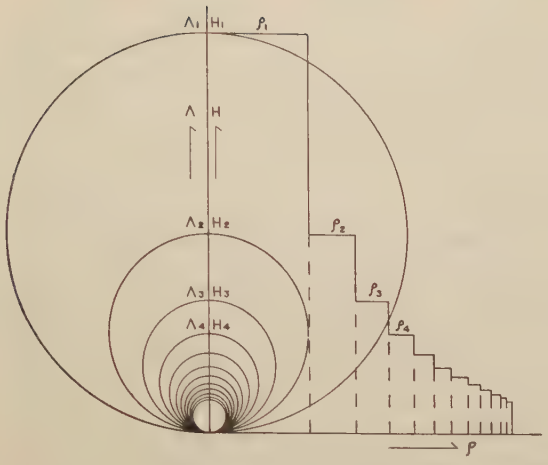

Fig. 4. Schematic diagram showing the interrelation between the scale Λ and the density ρ of the space charge concentration. For example, 2nd rank of space charge concentration has the scale Λ_2 and the density ρ_2. H is the height of the concentration.

Table 2. Interrelation between the values of n, Λ, H and ρ.

Rank	n	1	2	3	4	.....	k
Scale	Λ	1	$\frac{1}{2}$	$\frac{1}{3}$	$\frac{1}{4}$	.....	$\frac{1}{k}$
Height	H	1	$\frac{1}{2}$	$\frac{1}{3}$	$\frac{1}{4}$	.....	$\frac{1}{k}$
Space charge density	ρ	1	$\frac{1}{2}$	$\frac{1}{3}$	$\frac{1}{4}$	.....	$\frac{1}{k}$

$$Q=\frac{4}{3}\pi\left(\frac{\Lambda}{2}\right)^3\rho\,, \tag{7}$$

where a region of a sphere is available for three dimentional model. Then the electrostatic energy is given by

$$U=\frac{1}{2}\frac{Q^2}{\Lambda}. \tag{8}$$

From (7) and (8)

$$U\propto\rho^2\Lambda^5\,. \tag{9}$$

Substituting (6) into (9),

$$U\propto\Lambda^7\,, \tag{10}$$

that is,

$$U\propto n^{-7}\,. \tag{11}$$

This indicates that the energy spectrum of the atmospheric electric field follow the negative seventh power law.

In order to apply these considerations to the preceding experimental results, the electric field on the ground due to the space charge concentration of any rank should be considered. At the point of contact with the surface of the sphere on the earth's surface, the electric field intensity is

$$E=\frac{2Q}{\left(\frac{H}{2}\right)^2}. \tag{12}$$

Substituting into (8) and referring to (5),

$$U\propto E^2\Lambda^3. \tag{13}$$

From (10) and (13)

$$E^2\propto\Lambda^4, \tag{14}$$

or

$$E^2\propto n^{-4}. \tag{15}$$

This is in agreement with the above analytical result of January 10, 1956.

To see the order of the value of the actual scale, 2 or 3 km which corresponds to the height of the upper boundary of the exchange layer should be used as the value of the largest scale Λ_1 corresponding to the first rank. For example, as a scale of 6th rank it results in about 400–500 m. It is seen in Fig. 3 that in the lowest 500 m of the atmosphere there is an layer where $R_i<1$, during the period of January 8–13 except January 12, and the space charge configuration in this lowest unstable layer may be the cause of the great fluctuations at higher terms in the spectra in Fig. 2; that is, the space charge concentrations with smaller scales than 500 m are apt to be influenced by the turbulent situation of the air in the lowest levels of the atmosphere.

4. Concluding Remarks

The analytical results discussed above have been limited to the measurements obtained during only successive six days and may be not conclusive, some matters remaining to be confirmed in future. However, the results deduced in this paper may have an important meaning for the description of the atmospheric electric field; that is, the atmospheric electric field will be sufficiently understood by considering its perturbation which may be missed in the statistical method. Therefore, just as the daily curve of change derived from the statistical procedure is a very important measure of the atmospheric electric field, so is the spectrum derived in this paper perhaps another important measure. From this point of view, whether an observed atmospheric electric field would be returned to the fair weather or the non-fair weather, would be due to the value of the power of the spectrum.

The results discussed in the present paper show how the stability of the air in the lower levels of the atmosphere can control the atmospheric electric field. To obtain the better understanding of the atmospheric electric situation, Israël (1958) gave the concept of the "agitation" which is related to the atmospheric process within one hour, and he found that the agitation should be connected with the atmospheric turbulence. As to the relation between the atmospheric turbulence and the perturbation in the atmospheric electric field, a more detailed discussion will be given in a later paper.

The results are encouraging to understand the three dimentional structure of the atmospheric electric field, which may be regarded as a "turbulent field" consisting of various ranks of space charge concentration characterized by its own scale and its own density.

Aknowledgement

The author wishes to express his sincere thanks to Prof. Y. Tamura for his kind guidance and encouragement throughout the work, and also wishes to thank Mr. A. Okawati for his co-operation in the experimental program. Many thanks are also due to Dr. H. Maeda, Mr. K. Sakurai and Mr. S. Saga for their valuable discussions.

References

Dolezalek H. (1958) Recent Advan. Atmos. Electr. Pergamon Press, London 195.
Israël H. (1955) Proc. Conf. Atmos. Electr. Geophys. Recer. Pap. 42, (AFCRC), 11.
Israël H. (1958) Recent Advan. Atmos. Electr. Pergamon Press, London 149.
Kasemir H.W. (1950) Arch. Met. Wien. A 3, 84.
Sagalyn R.C. (1958) Recent Advan. Atmos. Electr. Pergamon Press, London 21.

$\gamma \rightarrow \alpha$ Transition in Fe_2O_3 with Pressure

By Ikuo KUSHIRO

Geological Institute, University of Tokyo

(Read May 16, 1960; Received May 20, 1960)

Abstract

The temperature of transition of synthetic γ-Fe_2O_3 (maghemite) to α-Fe_2O_3 (hematite) is lowered by increasing pressure. The transition line is represented by the equation, $p=150-0.3T$, where p is pressure in bar and T is temperature in °C. The transition of Ti-bearing γ-Fe_2O_3 (titanomaghemite) needs higher pressure and temperature than that of pure γ-Fe_2O_3. From the experimental results, it is suggested that maghemite is formed only near the surface of the earth, probably at depths shallower than about 500 m of the crust.

Introduction

The transition of cubic γ-Fe_2O_3 (maghemite) to rhombohedral α-Fe_2O_3 (hematite) by heating has been examined by several investigators (Michel, 1937; Forrer, 1938; Chaudron and Michel, 1938; Pouillard, 1949; Bozorth, 1951 and Shibuya, 1951) and it is accepted that the transition occurs irreversibly at a certain temperature between 275 and 800°C at 1 atm. The large difference in transition temperature has been interpreted as a result of presence of minor elements in solid solution. On the other hand, the effect of pressure on the transition temperature has not been known yet. In this paper, the results of the writer's experiments on the γ-α transition of Fe_2O_3 in relation to pressure and temperature are presented.

Experimental Results and Discussions

The original material used for the experiment is synthetic pure maghemite which was kindly offered by Dr. S. Akimoto and Mr. K. Kobayashi of the Geophysical Institute, University of Tokyo. The lattice constant determined by 'Norelco' X-ray diffractometer is 8.334 ± 0.002 Å, which accords well with the average value for natural maghemite given by Basta (1959) (8.335 Å). The transition experiment was made by using an ordinary test-tube type hydrothermal quenching apparatus. The run was made with free access of water in the reactor. For the lower pressure runs, the low-pressure gauge was specially used. The phases present after a run was identified by the Norelco X-ray diffractomerter.

The experimental results are summarized in Table 1 and are shown graphically with a transition line in the pressure-temperature diagram of Fig. 1. The transition

Table 1. Results of transition experiments

Pressure (bar)	Temperature (°C)	Time (hour)	Phases present
690	415	23	hematite
415	225	8	〃
275	162	14.5	〃
275	127	13.5	〃
160	351	12.5	〃
140	162	21.5	〃
105	130	17	maghemite
70	313	21.5	hematite+maghemite
70	250	24	maghemite
55	300	24	hematite+maghemite
35	477	22	hematite
35	236	10	maghemite
20	300	10	〃
1	570	0.1	hematite
1	530	24	hematite+maghemite
1	490	5	maghemite

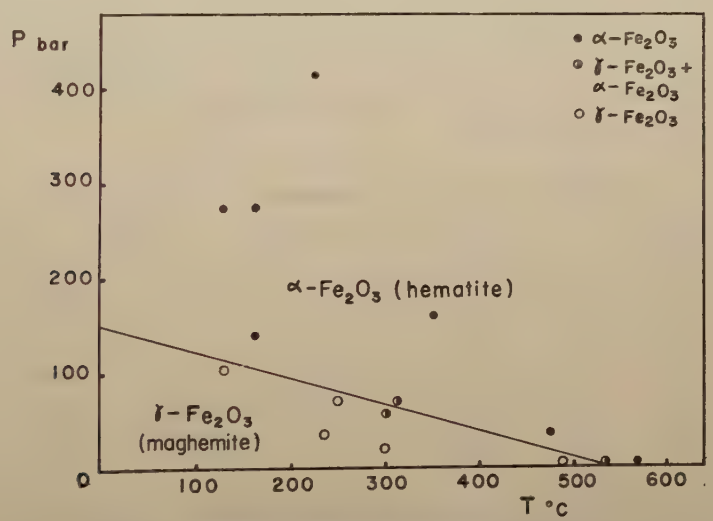

Fig. 1. Pressure-temperature diagram showing $\gamma \rightarrow \alpha$ transition in Fe_2O_3.

line is represented by the equation, $p=150-0.3T$, where p is pressure in bar and T is temperature in °C. The accuracy in the pressure and temperature measurements is not certain and there may be fairly large errors especially in the pressure measurement. Therefore the transition line given above has some uncertainty. As shown in the figure, the transition temperature is greatly affected by pressure. It is below 200°C at pressures higher than 100 bars. The reverse transition from hematite to maghemite has not been observed to occur. It was examined by keeping synthetic hematite at 200°C and 60 bars for 50 hours and at 380°C and 1 bar for 14 hours. Probably, maghemite is a metastable form of Fe_2O_3 and the transition from maghemite to hematite is irreversible.

For comparison, the behavior of Ti-bearing γ-Fe_2O_3 (titanomaghemite) was examined. As the starting material, natural titanomaghemite from the Atumi dolerite, Yamagata Prefecture (Sp. No. 1003) was used. The composition determined by T. Katsura is as follows; FeO: 11.89, Fe_2O_3: 56.53, TiO_2: 22.63, MgO: 0.45, MnO: 2.29, V_2O_3: 0.73, Al_2O_3: 1.94 in wt. %. It is situated near the $TiFeO_3$ (ilmenite)-Fe_2O_3 (hematite) join in the system TiO_2-FeO-Fe_2O_3. The lattice constant is 8.365 ± 0.002 Å. The experiment was done by the same method as that in the case of maghemite. Transition of the titanomaghemite to titanhematite did not occur even at higher pressure, but a decrease in lattice constant was observed. The results are listed in Table 2. The decrease in lattice constant, i.e. the decrease in unit cell volume, of titanomaghemite may be attributed to an existence of vacancies in the metallic position. This is supported by another experiment by which it was found that titanomagnetite from the Atumi dolerite (Sp. No. 1002) (FeO: 28.33 wt. %, Fe_2O_3: 44.18, TiO_2: 18.10) having less vacancies was less compressed (8.410→8.402 Å) than was No. 1003 at 2800 bars and 355°C. As shown in the table, the lattice constant ceases to decrease at higher pressure than 1200 bars, remaining almost at the same value of 8.344 Å. This may indicate that the degree of compression attained to the maximum at about 1200 bars. It was also found that the titanomaghemite is stable up to higher temperatures than the stability temperature of pure maghemite. The specimen No. 1003 did not change at 675°C and even at 840°C at ordinary pressure. The stability of titanomaghemite is probably a function of the Ti content: higher pressure and temperature may be required for the transition of maghemite with higher Ti content.

Table 2. Change in the lattice constant of titanomaghemite with pressure

Pressure (bar)	Temperature (°C)	Time (hour)	Lattice constant (Å)
3585	375	24	8.342
2760	330	20	8.345
1515	297	20	8.344
1200	330	16.5	8.344
760	330	16	8.349
585	221	22	8.358

The original specimen is titanomaghemite from the Atumi dolerite (Sp. No. 1003) whose lattice constant is 8.365 ± 0.002 Å.

From the experimental results, it is suggested that pure maghemite would not occur in the depths greater than about 500 m, below which transition to hematite would take place. Pure maghemite occurs in some magnetite deposits and is generally supposed to have been formed by oxidation of the latter mineral. By applying the results obtained from this experiment, the formation of magnetite may have occurred near the surface of the crust. On the other hand, titanomaghemite which is fairly common in igneous rocks (Akimoto and Kushiro, 1960) is stable over greater ranges of pressure and temperature. It would not invert to titanhematite even at considerable depth of the crust. The occurrence of titanhematite in some lavas as an oxidation product of titano-

magnetite may indicate that the oxidation took place at temperatures higher than about 900°C.

Acknowledgments

The writer is indebted to Prof. H. Kuno and Asst. Prof. A. Miyashiro for suggestions and critical reading of the manuscript. He is grateful to Dr. S. Akimoto and Mr. K. Kobayashi of the Geophysical Institute, University of Tokyo for providing synthetic maghemite and for helpful discussions, and also to Messrs. S. Aramaki and S. Banno of the Geological Institute, University of Tokyo for their valuable advices. Thanks are also due to Dr. T. Katsura of the Tokyo Institute of Technology for chemical analyses. A part of the expense of this study was defrayed from the Grant for Scientific Researches from the Ministry of Education.

References

Akimoto S. and Kushiro I. (1960) Jour. Geomag. Geoelectr. **11**, 94.
Basta E. Z. (1959) Econ. Geol. **54**, 698.
Bozorth R.M. (1951) Ferromagnetism.
Chaudron G. and Michel A. (1938) Comptes Rendus **208**, 90.
Forrer R. (1938) Comptes Rendus **207**, 670.
Michel A. (1937) Thèse, Paris 37.
Pouillard E. (1949) Thèse, Lille.
Shibuya G. (1958) Min. Jour. (in Japanese) **3**, 640.

Propagation of Low Energy Cosmic Ray Particles Associated with Solar Flares

By Kunitomo SAKURAI

Geophysical Institute, Kyoto University

(Read May 16, 1960; Received May 27, 1960)

Abstract

It has been observed that the low energy cosmic rays are produced associated with solar flares and propagate into interplanetary space. In this paper, we examined the features of the propagation mechanism of these cosmic rays, taking into account the results deduced from the theory of geomagnetic effect on these low energy cosmic rays. In consequence, we can conclude that the features of their incidence to the earth must have the impact zone effects, G.M.T. effects, and seasonal variations. Then, we examined the relations between these low energy cosmic ray events and solar and terrestrial phenomena in view of the observed data and made clear that both of flares and type IV outbursts taking place on western side of the sun seem to correlate these cosmic ray events much better. Taking into account those results we tried to explain reasonably the propagation mechanism of these low energy cosmic rays into interplanetary space and in addition to estimate the properties of magnetic clouds in that space.

1. Introduction

During the period of I.G.Y., the observations of low energy cosmic rays associated with solar flares were performed and through these observations it has been made possible to deduce the electromagnetic state between the sun and the earth. Such low energy cosmic rays associated with solar flares was observed firstly at the time of the great solar cosmic ray event on February 23, 1956 and it was found that the low energy part of solar cosmic rays continued to decay with very long tail during a few ten hours in the space around the earth (Winckler, 1956; van Allen and Winckler, 1956; Bailey, 1957; 1959). Thereafter, during the period of I.G.Y., it was often observed that low energy cosmic rays associated with solar flares impinge upon the geomagnetic high latitude regions and these observed results have been analyzed by many authors (Hakura, Takenoshita, and Otsuki, 1958; Anderson, 1959; Ney, Winckler, and Freier, 1959; Leinbach and Reid, 1959; Freier, Ney, and Winckler, 1959; Anderson, Arnoldy, Hoffman. Peterson, and Winckler, 1959; Hakura and Goh, 1959; Reid and Leinbach, 1959). From those analyses, it has been concluded that protons with energies from a few Mev to several hundred Mev, much smaller than those of the usual cosmic ray protons, are produced at the sun or its neighbourhood and they impinge upon the geomagnetic high latitude regions and that their incidence to the earth after solar flares seems to

have some relations to occurrences of the solar radio emission type IV outbursts and the geomagnetic storms with sudden commencement (Hakura and Goh, 1959; Reid and Leinbach, 1959). And then, it has been made clear that the flares which occurred on the western side of solar surface have better correlations with the incidence to the earth of the low energy cosmic rays than with those on the eastern side (Reid and Leinbach, 1959). Moreover, Hakura, Takenoshita and Otsuki (1958) performed the detailed analyses about the events of low energy cosmic ray incidence observed on September 13, 1957 and February 11, 1958 and made clear in detail the patterns of their incidence at the geomagnetic high latitude regions before the commencement and during the progression of geomagnetic storm. In order to investigate the propagation into interplanetary space of the low energy cosmic rays from the sun, the manner of their incidence to the earth, and the electromagnetic processes occurring in the earth's outer atmosphere in relation to the low energy cosmic ray events, such a work will be very important.

In this paper, we shall examine the propagation mechanism of the low energy cosmic rays associated with solar flares making use of data published by Hakura and Goh (1959), Reid and Leinbach (1959) and other workers, which were obtained during the period from June, 1957 to May, 1959. In section 2, we shall at first investigate the features of the incidence to the geomagnetic high latitude regions of the low energy cosmic rays coming from the sun's direction with the theory of geomagnetic effect on cosmic rays, and then show the results expected from the above calculations. Next, in section 3, we shall compare the results deduced from section 2 with the analyses by the authors quoted above, and examine the relationship between the incidence to the earth of such low energy cosmic rays and the solar and terrestrial phenomena associated with them, and consider their propagation mechanism into interplanetary space.

2. Motions of Low Energy Cosmic Rays in the Geomagnetic Dipole Field

It is known that the solar cosmic ray events observed five times in the past show the large fraction of cosmic ray particles arrive directly at the earth's neighbourhood from the sun and impinge upon the earth according to the expectation from theoretical calculations of the motions of cosmic rays in the geomagnetic dipole field, showing the so-called impact zone effects of their incidence (Firor, 1954; Lüst and Simpson, 1957). The energies of these cosmic ray particles which produce such events range from about 1 Bev to 30 Bev, but the energies of cosmic rays which we are going to examine here are much lower than the former, ranging from a few Mev to several hundred Mev. Thus, from the theory of geomagnetic effect of cosmic rays it is obvious that such low energy cosmic ray particles can only impinge upon the geomagnetic high latitude regions.

In this section, referring to the results of calculations by Malmfors (1945), Dwight (1950), Schlüter (1951; 1958), Firor (1954), Störmer (1955), Jory (1956), and Lüst (1956) and others and their methods of calculations, especially those of Störmer and Dwight, we shall examine the orbits of motion of cosmic ray particles with a few special rigi-

dities in the geomagnetic dipole field. The method of calculation is, roughly speaking, as follows;

At first, we assume that a cosmic ray particle impinges vertically upon the geomagnetic latitude λ. In Fig. 1, we shall show the directions of velocity vectors (λ_∞, φ_∞) which a cosmic ray particle arriving at λ will take before coming into the geomagnetic field.

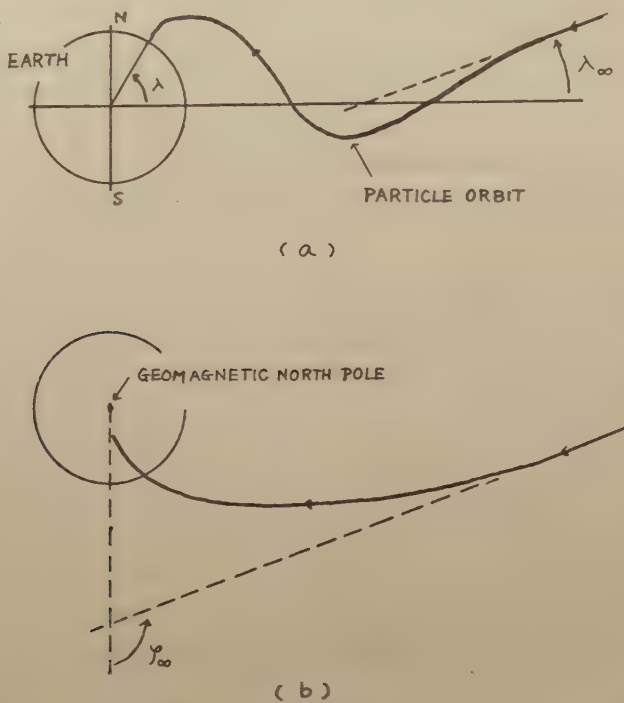

Fig. 1. Angle used to describe orbits of low energy cosmic rays coming from the sun and arriving vertically upon the earth, (from Firor (1954))
(a) orbit in a meridian plane that moves with particle, showing the latitude of incidence, λ, the latitude of the asymptotic velocity vector, λ_∞;
(b) projection of orbit on the equatorial plane. The angle φ_∞ is the longitude of impact relative to the source.

The results obtained from the calculations for the cosmic rays having special rigidities are shown in Figs. 2 and 3, where the results in respect to the particle rigidities 1, 2, and 3 Bev are reproduced from the calculations obtained by Firor (1954).

In the following, we shall examine the results which are obvious from the above calculations:

(1) Though the geomagnetic latitudes for the incidence of low rigidity particles shift to the much higher latitudes than those of general cosmic rays as shown in Fig. 2, Fig. 3 shows that φ_∞, i.e. the longitudinal component of the velocity vectors, is almost independent of particle rigidities. From this fact, it may be expected that such

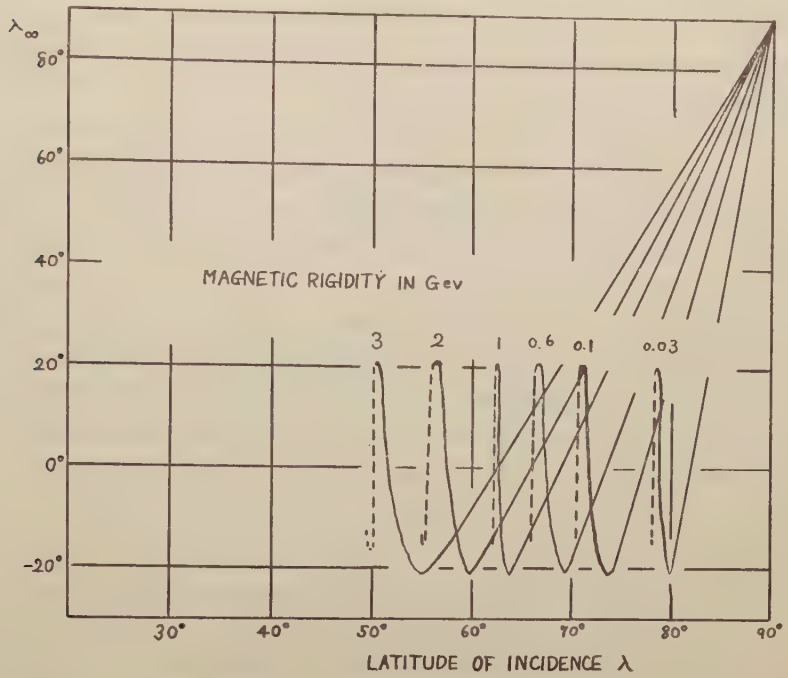

Fig. 2. Relation between the geomagnetic latitude of impact on the earth of particles arriving from the sun with magnetic rigidities of 30 Mev to 3 Bev, and the geomagnetic latitude of source.

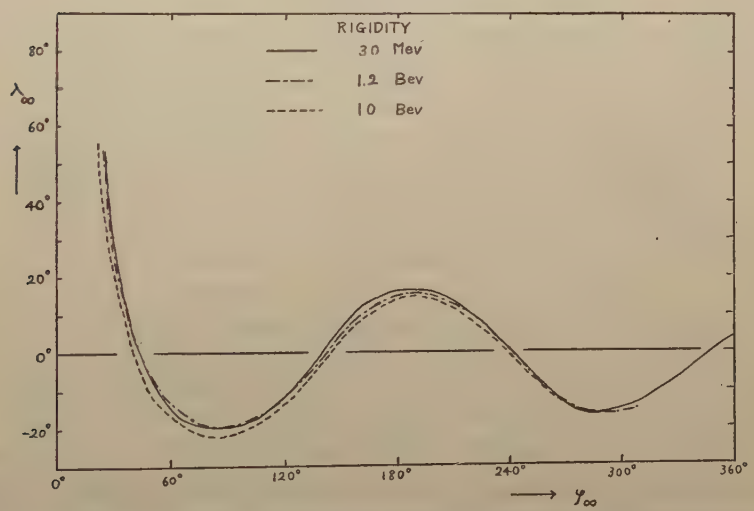

Fig. 3. Relation between the geomagnetic longitude of impact on the earth of particles arriving from the sun with magnetic rigidities of 30 Mev, 1.2 Bev, and 10 Bev, and the latitude of the source.

low energy cosmic ray particles impinging upon the high latitude regions will show anisotropic properties at the initial stages of their incidence to the earth, i.e., the existence of the impact zones and of background ones. Therefore, it can be supposed that there is a local time dependence on the incidence of low energy cosmic rays associated with solar flares.

(2) At the higher latitude regions, since the geomagnetic axis does not coincide with the geographic one, it seems that a Greenwich time dependence of their incidence to the earth appears in addition to the effect (1).

(3) The apparent position of the sun viewed from an observatory on the earth varies with the earth's rotation and revolution. Thus, as the apparent position varies annually, the source direction of the low energy cosmic rays, which is now equivalent to λ_∞, the latitudinal component of velocity vectors, will vary in the same manner. Therefore, it may be expected that there is the seasonal variation for the incidence frequency of the low energy cosmic rays associated with solar flares. As an example for the above expectation, we shall show in Fig. 4 the case of American zone, the region near about geographic 70 degrees West meridian in the north hemisphere. Since $|\lambda_\infty|$ of hatched area is greater than 20 degrees, the low energy cosmic rays associated with solar flares will not be observable in the American zone if this zone is in that area.

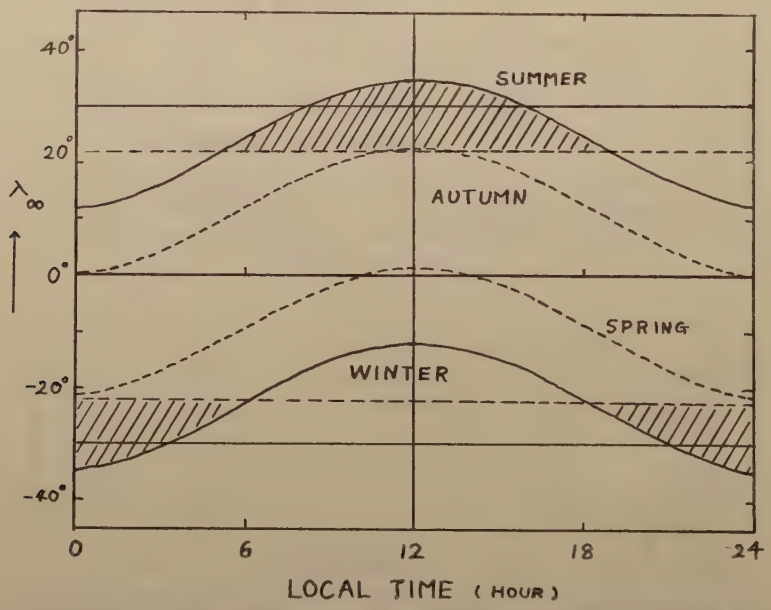

Fig. 4. Relation between the local time in the American zone and the apparent latitude of the sun, i.e. the source of low energy cosmic rays.

On the other hand, although the observed results show that low energy cosmic rays seem to impinge nearly isotropically upon the geomagnetic high latitude regions (Reid and Leinbach, 1959), it will be necessary to investigate in more detail the observational data in order to make clear whether or not the incidence of such low energy cosmic rays coincides with the expectation from the calculations. Furthermore, whether or not the seasonal variations of their incidence mentioned in (3) are existent is not yet confirmed.

At present, from that there is very great disagreement between the theory on the incidence of solar cosmic ray particles in the energy 1–30 Bev and the observations of these events having occurred in the past, it is estimated that these solar cosmic ray

particles are influenced very severely in their passage to the earth by the magnetic fields supposed to be existent in interplanetary space (see for example, Simpson, 1957; 1958). Namely, it is regarded as very plausible that those interplanetary magnetic fields play an important role on the anisotropy degrees of solar cosmic ray incidence to the earth and make these solar cosmic rays to impinge upon the higher latitudes. Therefore, if we suppose that the propagation directions of such low energy cosmic ray particles as treated in this paper are disturbed considerably in the passage from the sun to the earth by the influence of those interplanetary magnetic fields, it may be expected that those low energy cosmic ray particles impinge isotropically upon the earth from the initial stage of their incidence. Although most of the low energy cosmic ray events continue for very long time, say several ten hours (Table I), it can not be expected that these long time durations of their incidence are produced by the continuation of the solar production of low energy cosmic rays, because the associated flares continue at most during an hour. Consequently, there may be the mechanism which can trap these low energy cosmic rays for very long time in the solar neighbourhood or in the space between the sun and the earth and make them impinge upon the earth gradually.

3. Associated Phenomena and the Propagation into Interplanetary Space

If there is no magnetic field in interplanetary space, or if magnetic fields if any have configurations not affecting propagation of these low energy cosmic rays associated with solar flares, their incidence on the earth is to accord with the expectation obtained in section 2. So, we can expect that these low energy cosmic ray particles impinge predominantly upon the morning hemisphere of the earth. We may find out the above expectation in the work by Hakura et al. (1958), who investigated the low energy cosmic ray events on September 13, 1957. At present, since the investigations on the anisotropies of their incidence to the earth during a few hours after the beginning of their incidence have not been done in detail, we must say that our theoretical results concerning their incidence can not yet be confirmed. Therefore, in this section we shall not discuss in detail the features of their incidence to the earth, but examine the relationships among the productions of low energy cosmic rays at the sun, related solar phenomena and terrestrial ones, and thereafter, we consider the propagation mechanism of these cosmic rays into interplanetary space.

A. Analyses of Observational Data

Data used here were obtained in the period from June, 1957 to May, 1959 (Hakura, 1959; Hakura and Goh, 1959; Reid and Leinbach, 1959). At first, we show in Fig. 5 the positions of solar flares connecting with the production of low energy cosmic rays. In this figure, the type IV outbursts associated with flares producing these low energy cosmic rays and the ones not associated with these cosmic rays are also plotted together. We can see from this figure that the positions producing the incidence of low energy cosmic rays to the earth are mostly found on western side of the sun and that these flares are closely related with the occurrences of type IV outbursts and geomagnetic

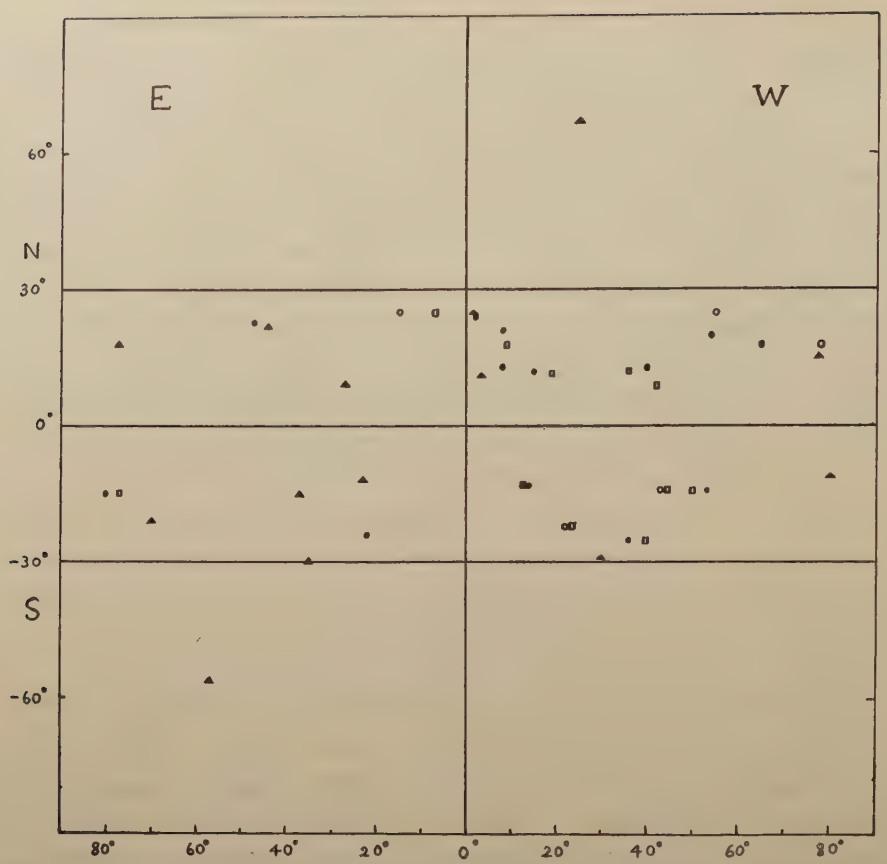

Fig. 5. Distributions of the solar flares producing the low energy cosmic ray events, and of type IV outbursts, shown on the heliographic map.

● : Flares associated with geomagnetic storms after low energy cosmic ray events.

○ : Flares not associated with geomagnetic storms after low energy cosmic ray events.

□ : Type IV outbursts connected with low energy cosmic ray events.

▲ : Type IV outbursts not associated with low energy cosmic ray events.

storms with sudden commencement. Now, it is also evident that type IV outbursts occurring on the eastern side of the sun have little correlation with the incidence of low energy cosmic rays to the earth. Consequently, we can see from the above results that there may be profound relationships among such connected phenomena as flares on western side of the sun, low energy cosmic ray events, type IV outbursts, and geomagnetic storms. And then, the more detailed analyses of observed data are shown in Table I and Figs. 6 and 7.

Table I shows the numbers of durations of their incidence to the earth by means of the time after flares. Fig. 6 (a) shows the frequency distribution of their incidence from occurrences of solar flares to the beginning of their incidence to the earth, which we show as ΔT. Fig. 7 shows the relations between the positions of flares shown with heliographic longitudes only and ΔT. Fig. 6 (b) shows time differences from occurrences of solar flares to the beginning of geomagnetic storms.

Table I.

The Durations of the Impingement Upon the Earth of Low Energy Cosmic Rays
(23 events are shown in this Table)

Duration (hrs)	Number of Events
0— 20	6
21— 40	6
41— 60	4
61— 80	3
81—100	4

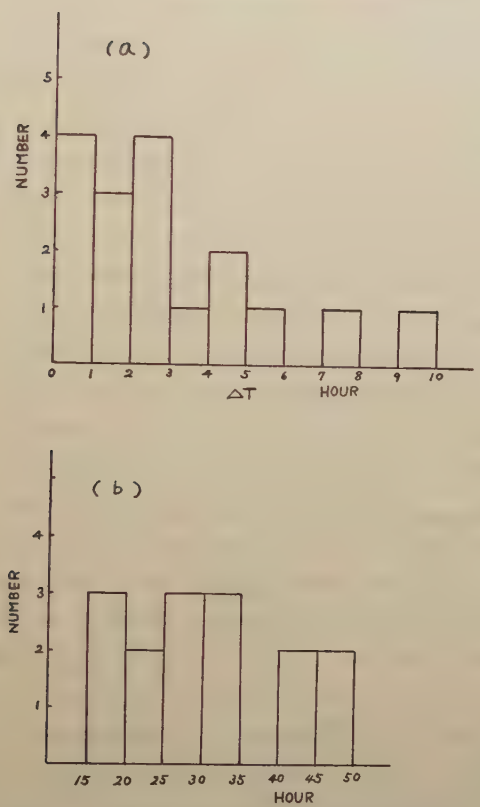

Fig. 6. Distributions of numbers of the time durations between solar flares and the beginning of low energy cosmic ray events, and of the time durations by the commencement of geomagnetic storms after solar flares.
(a) Time durations by the beginning of low energy cosmic ray events after solar flares.
(b) Time durations by the commencements of geomagnetic storms after solar flares.

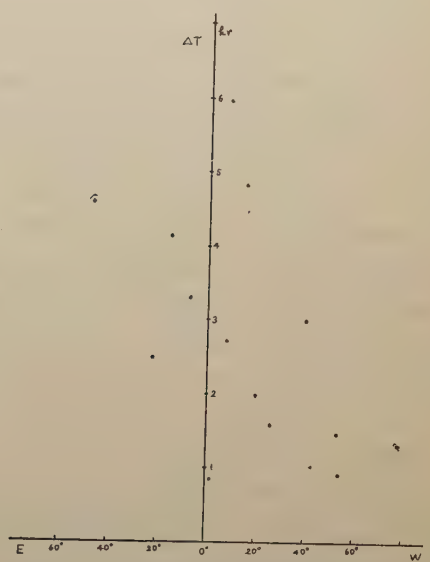

Fig. 7. Time intervals between the outset of solar flares and the beginning of impingement upon the earth of the low energy cosmic rays.

Since the sun-earth transit time along the straight line for these low energy cosmic rays, their main component being protons, produced at the sun with energies ranging from a few Mev to several hundred Mev, is at most some ten minutes, say about half an hour, it is certain from Fig 6(a) that by the influence of some mechanism the transit

time of these cosmic rays becomes much longer than that of their direct transit. Moreover, it is found from Fig. 7 that there is a tendency of the transit time becoming shorter and shorter as the positions of flares move more and more westwards on the sun. Thus, we can expect that these results obtained above give a very important clue to our consideration of the propagation mechanism of low energy cosmic rays through interplanetary space after their ejection from the sun. Finally, let us call attention to the continuation of their incidence during geomagnetic storms.

B. Propagation Mechanism

At present, it is well known that the cause of solar radio type IV outbursts is found in the relativistic electrons in solar outer corona (Boischot, 1957; Boischot and Denisse, 1957). The existence of large number of these high energy electrons above several Mev leads us to deduce that many protons with energies of the same order are present there. Therefore, we can conclude that these protons with energies ranging from a few Mev to several hundred Mev are produced near the sun at about the same time as occurrences of type IV outbursts and then they begin to propagate into interplanetary space. Thus, when these high energy protons leave the sun, the plasma clouds moving in the solar outer corona may, too, be ejected from the sun together with these protons, and afterwards begin to propagate as so-called magnetic clouds. Although we can conclude that both of low energy cosmic rays and magnetic clouds are ejected from the sun together into interplanetary space and thereafter they arrive near the earth, it seems, as we saw in subsection A, that there are some restrictions in the manner of the propagation of low energy cosmic rays. Therefore, taking into account these circumstances we must proceed to consider the mechanism in which low energy cosmic rays will already be affected very severely by the interplanetary magnetic fields before arriving near the earth since their incident directivities at the earth are very isotropical from the initial stage of their incidence (Reid and Leinbach, 1959). Both facts that the sun-earth transit time of them tends to being dependent on the heliographic positions of flares as can be seen from Fig. 7, and that as evident from Fig. 5 the heliographic positions of flares producing these low energy cosmic rays incline to western side of the sun, may give us the following conclusion: namely, when low energy cosmic rays propagate through interplanetary space their directivities of propagation are not disturbed at random, but such an electromagnetic state that these low energy cosmic rays produced on western side of the sun can approach the earth more easily than those on the other side may be existent in the space between the sun and the earth.

On the other hand, making use of cosmic ray data at Mt. Washington in the summers, 1957 and 1958, Towle and Lockwood (1959) performed the same investigation as the treatment by Firor (1954). who studied data in the period between 1951 and 1953, but they could not obtain such results as Firor's. Namely, they could not detect even smallest unusual increases of solar cosmic rays associated with small flares in the periods of 1957 and 1958. Accordingly, they suggest based on their investigation that the electromagnetic state in interplanetary space, into which solar cosmic rays propagate, varies in accordance with the secular variations of solar activity and that in the

periods of the solar activity maxima interplanetary magnetic fields may take such configurations as to disturbe violently the directivities of propagation of solar cosmic rays. So, referring to their investigation, we can suppose definitely the directivities of propagation of low energy cosmic rays treated in this paper through interplanetary space will be disturbed very violently by interplanetary magnetic fields. From the results obtained in this section and the consideration made by Towle and Lockwood (1959), we can deduce that there are magnetic irregularities affecting in the similar manner both of low energy cosmic rays with energies a few Mev- several hundred Mev and relatively high energy cosmic rays with energies of several Bev. It may be possible to explain reasonably why Towle and Lockwood (1959) could not detect any solar cosmic rays with several Bev energies, if we presume that the interplanetary magnetic field configurations are variable according to solar activity cycles and therefore in the periods of solar activity maxima the incident directivities of these solar cosmic rays to the earth are purely random by the influence of magnetic fields mentioned above, and that the production rate of these cosmic rays is much smaller than that of low energy cosmic rays. So, we may conclude with Towle et al. (1959) that since interplanetary magnetic fields in the declining periods of solar activity seem to be transparent to the solar cosmic ray propagation, such results as Firor's may be obtainable. Our explanation, however, is still unsatisfactory because the magnetic fields in interplanetary space deduced above indeed disturbe severely the incident directivities to the earth of low energy cosmic rays on the one hand, but on the other hand these fields have such properties as to maintain well their direction of propagation as a whole as shown in Fig. 5. Consequently, configurations of interplanetary magnetic fields must be able to explain these facts reasonably. If we refer as plausible to the magnetic fields in interplanetary space presented by Cocconi et al. (1958) and Parker (1958a, b), it may be favorable to our reasonable explanation of the low energy cosmic ray events associated with solar flares.

As evident in Table 1, most of the low energy cosmic ray events continue to impinge upon the earth during very long time and during geomagnetic storms, too (Freier, Ney and Winckler, 1959; Reid and Leinbach, 1959). Since it is very difficult to explain such long duration of their incidence on the basis of the solar flare origin alone, a mechanism has been proposed, in order to explain it reasonably, in which these low energy cosmic ray particles, as being trapped in magnetic clouds ejected from the sun, propagate into interplanetary space together with magnetic clouds (Gold, 1959). Thus it may be very plausible there is two manners in the propagation mechanism of low energy cosmic rays. Our explanation of the propagation mechanism of low energy cosmic rays will be as follows; particles arriving at the earth before the beginning of geomagnetic storms are trapped in magnetic clouds when leaving from the sun and soon later diffuse out of them gradually, and most of the former propagate into interplanetary space along the radial magnetic fields of tongue type extended from the sun and those impinging upon the earth during geomagnetic storms arrive at the earth as being trapped in magnetic clouds. Moreover, the tail of their incidence remaining

after the end of geomagnetic storms may be produced by the leakage of particles trapped in magnetic irregularities near the sun.

C. Characteristics of Magnetic Clouds

It seems that magnetic clouds in which low energy cosmic rays are trapped will expand during the propagation into interplanetary space and their magnetic intensities will decrease gradually (Batchelor, 1955; Hirono, 1957).

In this subsection, taking into acount that magnetic clouds are able to trap these cosmic rays for a long time, we shall examine, though very rough, the intensities of magnetic fields and their dimensions. Since we can suppose the cosmic ray particles impinging upon the earth in the initial stages of these events as having escaped from the trappings by magnetic clouds in a few 10 minutes or several hours, we can estimate, with those observations, the order of magnetic intensities or dimensions of young magnetic clouds near the sun. And moreover, taking into acount trappings of low energy cosmic rays for several 10 hours in later stages, we can estimate the lower limits on these quantities of magnetic clouds in interplanetary space. The results obtained with various magnetic intensities are shown in Tables II and III. The

Table II.

Dimensions of Magnetic Clouds near the Sun deduced from Low Energy Cosmic Ray Events

Magnetic Field Intensity (Gauss)	Dimensions of Magnetic Clouds (cm)				
	0.5 hr*	1.0 hr	1.5 hr	2.0 hr	2.5 hr
10^{-3}	2.4×10^{11}	3.5×10^{11}	4.1×10^{11}	4.2×10^{11}	5.4×10^{11}
10^{-4}	7.2×10^{11}	1.0×10^{12}	1.3×10^{12}	1.5×10^{12}	1.6×10^{12}
10^{-5}	2.4×10^{12}	3.5×10^{12}	4.1×10^{12}	4.2×10^{12}	5.4×10^{12}

*; Time necessary to escape from magnetic clouds

Table III.

Dimensions of Magnetic Clouds in the Later Stages

Magnetic Field Intensity (Gauss)	Dimensions of Magnetic Clouds (cm)	
	24 hr	48 hr
10^{-3}	1.59×10^{12}	2.3×10^{12}
10^{-4}	5.02×10^{12}	7.26×10^{12}

methods of calculations used here are as follows: we shall assume that low energy cosmic rays can escape by diffusion from magnetic clouds. Thus, the diffusion constant in these clouds are given as $D=\frac{1}{3}lv$, where l is transport mean free path and v is particle velocity. We assume l as equal to the spiral radius of a charged particle with energy E (ev units) in magnetic field (Gauss units), that is, $l=\frac{E}{300.}$ Consequently, because time necessary to escape from magnetic clouds by diffusion is known from the observations, the dimensions of magnetic clouds (L) are,

$$L \approx \sqrt{D\tau} \text{ (cm)},$$

where τ is the time of escape above mentioned. Thus, we may obtain the dimensions of magnetic clouds, where in these estimations we assume $E=10$ Mev as representative.

Although the dimensions of magnetic clouds in this subsection are much smaller than those considered usually at present, these values are near those estimated by Hirono (1957).

4. Concluding Remarks

In section 2, we examined the motions of low energy cosmic ray particles in the dipole magnetic field of the earth and described some results expected from those examinations. Since the features of the incidence to the earth of those cosmic rays, however, have not yet been investigated in detail, we can not decide at present whether or not those particles show a tendency of impinging upon the earth in accordance with the expectations from theoretical calculations. We must, therefore, examine, in order to make clear the above mentioned problems, the manner of the incidence of these cosmic rays, taking into account observed data and referring to theoretical results. In section 3, we discussed on both the solar and terrestrial phenomena occurring in connection with low energy cosmic rays associated with solar flares and showed that the arrival of these low energy cosmic rays at the earth has some relations with flares on western side of the sun, and that positions of type IV outbursts related with those events incline to western side. These facts seem to be favorable to the explanation that these low energy cosmic rays propagate into interplanetary space along the radial magnetic fields of tongue type extended from the sun and dragged somewhat by the solar rotation. It is estimated that in the propagations of these cosmic rays is included so-called indirect method propagation (Gold, 1959) of them trapped in magnetic clouds.

Acknowledgement

The author wishes to express his sincere thanks to Prof. Y. Tamura and Prof. M. Hasegawa for their kind advice and encouragement, and Prof. K. Maeda for his valuable discussions and criticisms on this work. His thanks are also due to Dr. H. Maeda and Dr. Y. Hakura for their kind advice and suggestions.

References

Anderson K. (1959) Phys. Rev. Lett. **1**, 335.

Anderson K., Arnoldy R., Hoffman R., Peterson L. and Winckler J.R. (1959) J. Geophys. Res. **64**, 1133.

Bailey D.K. (1957) J. Geophys. Res. **62**, 431.

Bailey D.K. (1959) Proc. IRE. **47**, 255.

Batchelor G.K. (1955) Gas Dynamics of Cosmic Clouds, p. 117, ed. by Burgers J.M. and van de Hulst H.C.; North Holland Publ.

Boischot M.A. (1957) Compt. Rend. **244**, 1326.

Boischot M.A. and Denisse J.F. (1957) Compt. Rend. **245**, 2194.

Cocconi G., Gold T., Greisen K., Hayakawa S. and Morrison P. (1958) Nuovo. Cim. Supp. **8**, Ser 10, 161.

Dwight K. (1950) Phys. Rev. **78**, 40.

Firor J. (1954) Phys. Rev. **94**, 1017.

Freier P.S., Ney E.P. and Winckler J.R. (1959) J. Geophys. Res. **64**, 685.

Gold T. (1959) J. Geophys. Res. **64**, 1665.

Hakura Y., Takenoshita Y. and Otsuki T. (1958) Rep. Ionos. Res. Japan **12**, 459.

Hakura Y. (1959) Uchusen-Kenkyu **4**, 50 (Journal of Cosmic Ray Research in Japanese).

Hakura Y. and Goh T. (1959) J. Radio Res. Lab. **6**, 635.

Hirono M. (1957) Rep. Ionos. Res. Japan **11**, 205.

Jory F.S. (1956) Phys. Rev. **103**, 1068.

Leinbach H. and Reid G.C. (1959) Phys. Rev. Lett. **2**, 61.

Lüst R. (1957) Phys. Rev. **105**, 1827.

Lüst R. and Simpson J.A. (1957) Phys. Rev. **108**, 1563.

Malmfors K.G. (1945) Ark. Mat. Astr. Fys. **32A**, 1.

McLean D.J. (1959) Austr. J. Phys. **12**, 404.

Ney E.P., Winckler J.R. and Freier P.S. (1959) Phys. Rev. Lett. **3**, 183.

Parker E.N. (1958a) The Plasma in a Magnetic Field, p. 77, ed. by Landshoff R.K.M.; Stanford Univ. Press.

Parker E.N. (1958b) Ap. J. **128**, 664.

Reid G.C. and Leinbach H. (1959) J. Geophys. Res. **64**, 1801.

Schlüter A. (1951) Zs. f. Naturforsch. **6a**, 613.

Schlüter A. (1958) Nuovo. Cim. Supp. 8, Ser 10, 349.

Simpson J.A. (1957) Proc. Natl. Acad. Sci. **43**, 42.

Simpson J.A. (1958) Nuovo. Cim. Supp. 8, Ser 10, 133.

Störmer C. (1955) Polar Aurora.; Oxford Clarendon Press.

Towle L.C and Lockwood J.A. (1959) Phys. Rev. **113**, 641.

van Allen J.A. and Winckler J.R. (1956) Phys. Rev. **106**, 1072.

Winckler J. R. (1956) Phys. Rev. **104**, 220.

Types of Diurnal Variation of the Air-Earth Current

By Toshio OGAWA

Geophysical Institute, Kyoto University

(Read May 16, 1960; Received May 29, 1960)

Abstract

The daily percentage variations of the air-earth current were calculated every longitude of 90° over the world, using the percentage variation of the potential of the upper conducting layer (atmospheric total potential) deduced from *Carnegie* measurements over the oceans, and that of the columnar resistance obtained from the measurements by Sagalyn and Faucher. The results generally represent the world-wide distribution of the measured daily variation curves which were arranged by Israël. This fact generally indicates that the daily percentage variations of the columnar resistance at the most stations over the land area are roughly equal, and also of the same magnitude as the universal daily percentage variation of the atmospheric total potential. However, more detailed discussions by comparing the measured and the calculated results at the urban district of the meridian 135° *E* show that the daily variations of the air-earth current depend more on the local columnar resistance than the atmospheric total potential, the percentage variation of the former being twice as much magnitude as that of the latter. It is suggested that at the urban district the unclei concentration in the lowest layer of the exchange layer plays an important part in the atmospheric electric current system.

1. Introduction

The air-earth conduction current in the atmosphere has been considered to be of fundamental importance in the atmospheric electricity. The reason is as follows. First, the quasistatic state of the atmospheric electricity gives the constant value of the air-earth conduction current density with altitude from the upper conducting layer to the earth; thus the time variation of the air-earth current has been expected to be an important clue to indicate the time variation of the potential of the upper conducting layer with respect to the earth. Second, the air-earth current depends on the atmospheric total potential and the columnar resistance and they will be both less subjected to variations than the potential gradient and the conductivity; so the air-earth current will be less subjected to variations with time of day. Thus, the air-earth current has also been expected to be less influenced by local effects; local changes of conductivity can alter the air-earth current only to the extent to which they alter the tolal columnar resistance. These should be experimentally confirmed.

Although the statistical method has shown the characteristic definite types of daily

variation of the potential gradient, the air-earth current does not seem to tend toward definite types of variation but give rather divergent character. Mühleisen (1956) pointed out that the air-earth current is greater in the daytime than at night, in spite of the increasing of the columnar resistance in the daytime. He has concluded that the positive space charges which enlarge the primary field in the lowest air layers must be considered. Though the space charge effects must be certainly taken into considerations, they do not cause the divergent character of variation of the air-earth current only by themselves.

The daily variation of the potential of the upper conducting layer depends on the Greenwich Mean Time and that of the columnar resistance depends on the local time. As the air-earth current is related to those two factors, the daily variation of the air-earth current should depend on the longitude. Therefore, the fundamental types of variation to be in any longitude of the world should be considered. And also it should be examined that which the daily variation of the air-earth current at every location of the world depends on more the atmospheric total potential or the columnar resistance.

2. Longitude Distribution of the Types of Diurnal Variation of the Air-Earth Current

The air-earth current can be measured by two different methods. The actual air-earth current can be measured directly, and also it is possible to give the air-earth conduction current indirectly by measuring the local potential gradient and the local conductivity independently. The air-earth conduction current density i is related to the potential gradient E and the conductivity λ by

$$i=\lambda E. \tag{1}$$

On the other hand, the air-earth conduction current density is also given by

$$i=\frac{V}{R}, \tag{2}$$

where V is the potential of the upper conducting layer and R is the columnar resistance. Though it is not possible to measure directly the atmospheric total potential and the columnar resistance, the values and the variations of these quantities can be deduced indirectly as to be mentioned below.

The time variation of the air-earth current is given by differentiation of the equations (1) and (2) as

$$\frac{1}{i}\frac{di}{dt}=\frac{1}{\lambda}\frac{d\lambda}{dt}+\frac{1}{E}\frac{dE}{dt}, \tag{3}$$

and

$$\frac{1}{i}\frac{di}{dt}=\frac{1}{V}\frac{dV}{dt}-\frac{1}{R}\frac{dR}{dt}; \tag{4}$$

that is, the time variation of the air-earth current deinsity is sufficiently represented

by the percentage variations of E and λ, or V and R without considering their absolute values.

Israël (1954) has arranged the diurnal curves of the air-earth current at 10 stations in the world according to the geographic latitude, which are reproduced in Fig. 1. Between all of them he could not find out any common feature depending on either the universal time or the local time. Thus the systematical explanation of such diurnal curves has not yet been given.

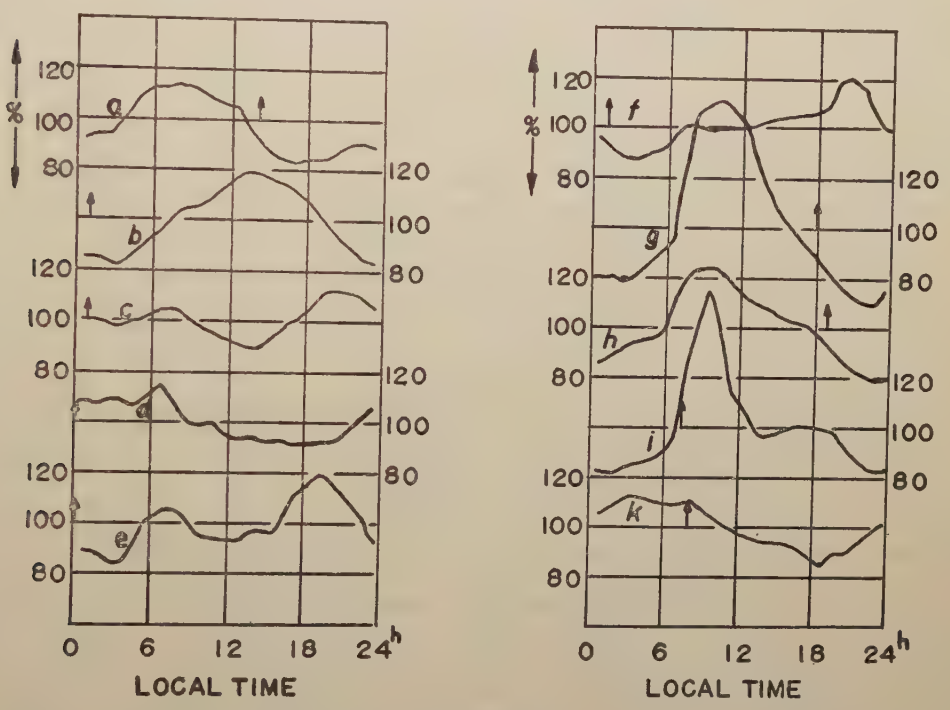

Fig. 1. Mean diurnal variations of air-earth current density in percentage (obtained during the period of one year at least) at the stations

a) Fairbanks/Alaska (Gish and Sherman, 1940)
b) Uppsala (Benndorf and Hess, 1928)
c) Potsdam (Kähler, 1909)
d) Kew (Scrase, 1933)
e) Chambon-la-Forêt (Institute de Physique du Globe, Paris)
f) Buchau (Israël, 1954)
g) Tucson (Wait and Torreson, 1941)
h) Huankayo (Peru) (Torreson and Wait, 1948)
i) Bandoeng/Java (Leckie, 1938)
k) Watheroo/Westaustralien (Wait and Torreson, 1941).

The stations were arranged according to the geographic latitude. The arrows on the abscissas give 0^h GMT. (after Israël, 1954)

In the equation (4), if the percentage variation of R is negligibly small compared with that of V, the percentage variation of i is the same as that of V and must depend on the Greenwich Mean Time. While, if the percentage variation of V is negligibly small compared with that of R, the percentage variation of i undergoes the change in the opposite sense to R and must depend on the local time. However the world-wide

distribution of the diurnal curves of the air-earth current given by Israël indicates that neither the percentage variation of the atmospheric total potential nor that of the columnar resistance are negligible and the two quantities are both quite effective on the variation of the air-earth current; the author sees the coupling effect of the two quantities in the Israël's empirical results.

The potential of the upper conducting layer cannot be directly measured, but it is possible to estimate the potential from the measured potential gradient distribution with altitude by integrating from the earth to the upper conducting layer. This is given by

$$V=-\int_0^H Edh, \tag{5}$$

where H is the height of the presumed upper conducting layer. Clark (1958) estimated the mean potential of 290 kV from the measurements between 0.015 km and 6 km above locations from Greenland to Key West by an airplane.

From the equations (1) and (2), the potential gradient is shown by

$$E=\frac{1}{\lambda}\frac{V}{R}. \tag{6}$$

By differentiating (6), the time variation of the potential gradient is given by

$$\frac{1}{E}\frac{dE}{dt}=\frac{1}{V}\frac{dV}{dt}-\frac{1}{\lambda}\frac{d\lambda}{dt}-\frac{1}{R}\frac{dR}{dt}. \tag{7}$$

If λ and R are unaffected by time of day, then E shows the variation of V. These conditions are achieved over the ocean. In analysing the results obtained during the cruise of the *Carnegie*, Mauchly (1923) showed the variation of potential gradient over the ocean to be singly periodic with a maximum at about 19^h GMT, independent of the local time. The atmospheric total potential will vary diurnally in such a manner as is described by this variation. This is shown in Fig. 2.

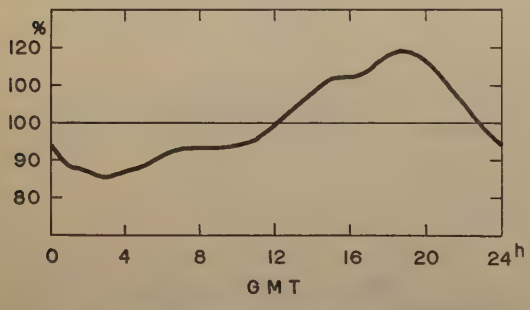

Fig. 2. Diurnal variation of atmospheric potential.

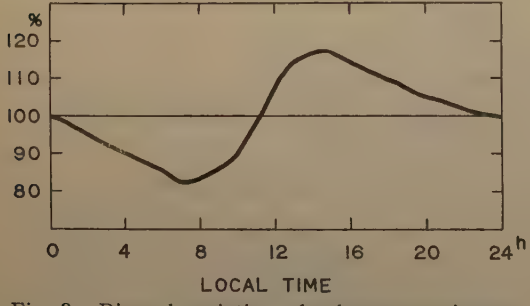

Fig. 3. Diurnal variation of columnar resistance over continents.

The columnar resistance is obtained by

$$R=\int_0^H \frac{1}{\lambda}dh. \tag{8}$$

The columnar resistance from the earth's surface to 15,000 ft was computed from the conductivity measurements over New Hampshire by Sagalyn

and Faucher (1956). The daily percentage variation of the average columnar resistance are given in Fig. 3. It is not proved whether the daily changes in the columnar resistance in any other locations over the land area are of the same order of magnitude in percentage as that in New Hampshire.

Using the percentage variation of the atmospheric total potential in Fig. 2 and that of the columnar resistance in Fig. 3, the diurnal percentage variations of the air-earth current can be calculated by the equation (4). The results are obtained every longitude of 90° and shown in Fig. 4, in which the arrows give 0^h GMT. It is interesting to see how representative the characteristic features in these diurnal curves of variation over the world are of those in the measured ones given in Fig. 1. The most characteristic feature in Fig. 4 is that there are two types of diurnal variation in the air-earth current. One is the double periodic variation with one maximum before and after noon respectively—curve *A*. The other type of variation is a single periodic one with a maximum in the morning and a minimum in the after noon—curves *B*, *C* and *D*. The double periodic type of variation has smaller amplitude in daily change than the single periodic one.

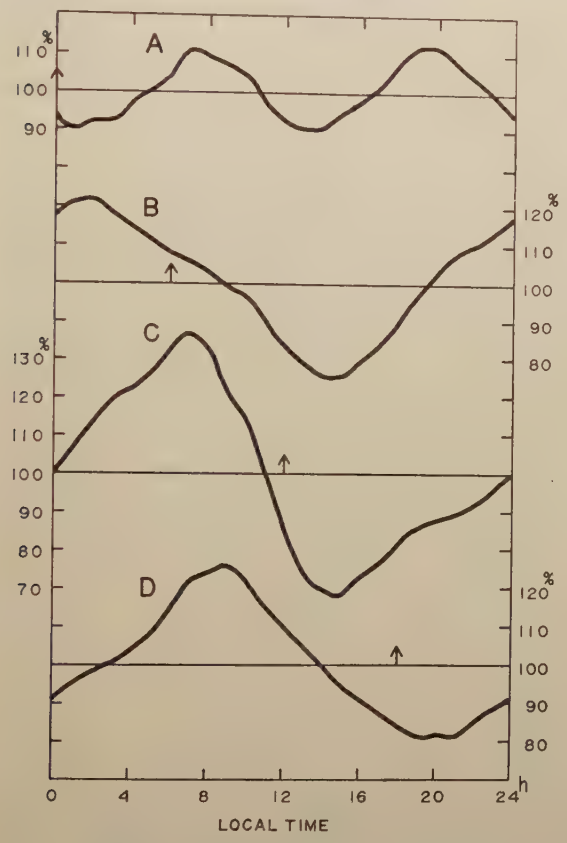

Fig. 4. Diurnal variations of air-earth current calculated on every longitude of 90°. The arrows give 0^h GMT.

In comparison between Figs. 1 and 4, the relations between the measured and the calculated variation curves of the air-earth current are shown in Table 1, in which the

Table 1. Relations between the calculated and the measured air-earth currents (Circles indicate good agreement and cross marks indicate poor agreement in the general features of the period and the amplitude.)

Calculated / Measured / Features	A (0°)					B (90°E)		C (180°E)	D (270°E)	
	b	c	d	e	f	i	k	a	g	h
Period	×	○	×	○	○	×	○	○	○	○
Amplitude	×	○	○	○	○	○	×	×	○	○

circles indicate good agreement between them in the general features of the period and the amplitude, while the cross marks indicate poor agreement. As the measured air-earth current may contain the effects of other generators than the thunderstorm generator and the columnar resistance used in the calculations may require some corrections at the respective stations, it is difficult to expect more excellent agreement between the two cases. From the general agreement of the calculated and measured air-earth currents, however, it can be pointed out that the diurnal percentage variations of the columnar resistance in any locations over the land area are roughly of the same order of magnitude as that in New Hampshire, and therefore the columnar resistance as well as the atmospheric total potential has an important role in the atmospheric electric current system over the land area.

3. An Example at the Urban District of the Meridian 135°*E*

In order to give more detailed discussions, the diurnal percentage variation of the air-earth current is calculated at the meridian 135°*E* (the standard meridian of Japan), using the above percentage variations of the atmospheric total potential and the columnar resistance in Figs. 2 and 3. The result is shown in Fig. 5, in which the time is referred to the mean local time of the meridian 135°*E*.

At the Geophysical Institute of Kyoto University, the potential gradient, polar conductivities and the wind velocity have been recorded on a recording paper. The Institute is located in the north-east district in Kyoto City which has the population of about one million and no big industrial area. Throughout the year and especially in the cold season, it is excelled in westerly wind over Kyoto. The generating voltmeter type field meter and the Gerdien type conductivity meters with the vibrating-reed electrometers are set atop the building 15 m high to avoid disturbances near the ground. Using the values of the measured potential gradient and conductivities, hourly values of the air-earth current are calculated on every day.

Although the potential gradient and the conductivity are largely subjected to local effects, they appear usually as a mirror image of the time variation of each other; so their product, that is, current density will be generally expected to be more indicative of universal effects. However the air-earth current thus obtained are very much modified by the short periodic fluctuations which are considered to be caused by the local effects. So far as two-dimensional structure of the atmospheric electric field is considered, such short periodic flucturtions in the air-earth current should not appear; three-dimensional irregularities of conductivity or space charge density should be the origins of these fluctuations, and these irregularities will be due to local effects. In order to eliminate these fluctuations due to local effects, the daily variation curves of the air-earth current are smoothed out by taking hourly the overlapping means of 5 hours over the interval 0^h–24^h on every fair-weather day. The results thus obtained are considered to be free enough from the local effects due to the local or Austausch generator to be analysed here. Thus the diurnal variations of the air-earth current on 6 days of fair weather in every month are obtained, and the mean diurnal variation

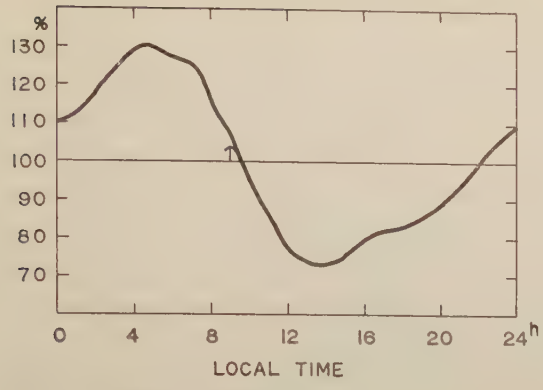

Fig. 5. Diurnal variation of air-earth current calculated in the longitude of 135°E. The arrow gives 0^h GMT.

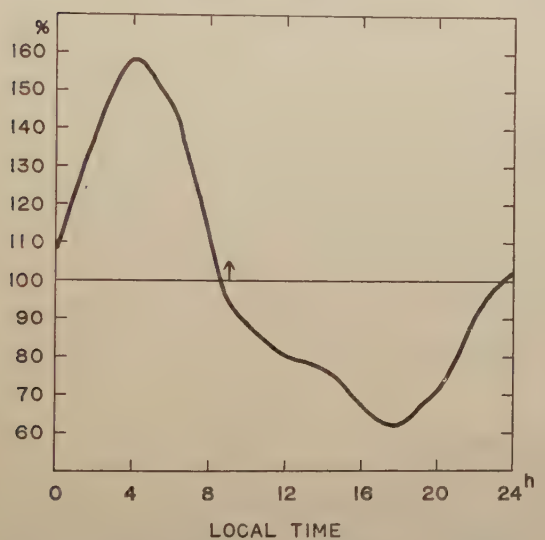

Fig. 6. Average diurnal variation of air-earth current obtained indirectly in Kyoto. The arrow gives 0^h GMT.

on every month are calculated. In Fig. 6, the average curve of variation of 4 months from September to December, 1959 is shown.

The most remarkable features in Fig. 6 are that the amplitude of the variation is about twice as that of the fundamental type of variation in Fig. 5, and the time of appearance of the minimum displaces toward later. Such differences can be summarized in terms of the columnar resistance in the atmospheric electric current system over the land area. Using the percentage variation of the atmospheric total potential in Fig. 2, the diurnal percentage variation of the columnar resistance can be calculated. The result is shown in Fig. 7, which represents the characteristic features of the columnar resistance at the urban district.

The result is compared with the columnar resistance in Fig. 3. In the first place, the amplitude of the variation is about twice as that in Fig. 3. This shows the daily variation of the columnar resistance to be about twice as much magnitude as that of the atmospheric total potential. Second, the time of occurrence of the minimum in the morning is 4^h and the substantial increasing begins at about 6^h, while the minimum appears at 7^h in Fig. 3. This difference will depend on the degree of the urban conditions over the land area. In urban districts, the increasing of the columnar resistance is caused by the accumulation of the unclei in the lowest layer of the exchange layer, while in rural districts, it is the result of conveyance of the nuclei from the urban districts. It results in the difference of the time of the occurrence of the increasing of the columnar resistance. Third, the time of occurrence of the maximum in the afternoon is 18^h, while it appears at 15^h in Fig. 3. This is related to the mechanism of the daily change in the atmospheric electric field, which will be described in a later paper.

Early in the morning before the sunrise when atmospheric state is the most stable,

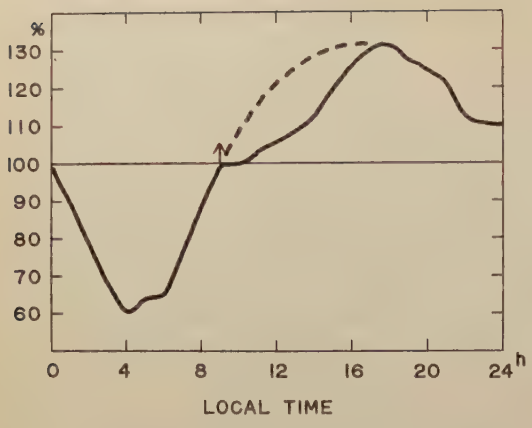

Fig. 7. Average diurnal variation of columnar resistance deduced from Figs. 2 and 6. Dashed line represents the case without horizontal diffusion of nuclei. The arrow gives 0^h GMT.

in urban districts, the conductivity at the earth's surface begins to decrease by the production of man-made nuclei which accumulate in the lowest layer of the exchange layer. It results in the increasing of the columnar resistance. In the daytime when the convection becomes stronger and the wind begins to blow, the turbulent mixing occurs and destroys the nuclei accumulation in the lowest layer. The nuclei are brought up into the upper layers in the exchange layer, and at the same time they are diffused horizontally. As the results slackens the increasing of the total resistance of an air column of unit area in horizontal cross section. The effect of this mechanism can be seen from 9^h to 17^h in Fig. 7. The columnar resistance presumed to be unaffected by the horizontal diffusion of nuclei is represented by the dashed line in the figure. In comparison between Figs. 3 and 7, the maximum at 15^h in Fig. 3 falls in the interval of this dashed line in Fig. 7; the maximum of the columnar resistance in rural districts depends on the horizontal conveyance of the nuclei produced at the sources in urban districts. The distribution of daily variation of the columnar resistance with distance from the sources of nuclei should be investigated.

4. Concluding Remarks

According to Kraakevik (1958), the air-earth conduction current density in the exchange layer is larger than that above the exchange layer on the average some 30%, due to upward convection of positive space charge. This is the effect of the local or the Austausch generator. About this generator Mühleisen (1958) has investigated in some details, but it is difficult to separate the effects of the local generator completely from the universal course of the atmospheric electric field due to the thunderstorm generator. As the effectiveness of the local generator changes from day to day and from time to time, it will be a promising method to take the overlapping mean hourly values over a day for seeing the mechanism of the daily changes in the atmospheric electric field as will be described in the later paper.

The results discussed in this paper are encouraging to understanding the daily variation of the air-earth current. However, as the variation types of the air-earth current are different at different longitude, it is hopeful to make close argument in many stations over the world.

Acknowledgement

The author wishes to express his sincere thanks to Prof. Y. Tamura for his kind guidance and encouragement throughout the work. He also wishes to thank Mr. S. Saga for his valuable discussions.

References

Clark J.F. (1958) Recent Advan. Atmos. Elect. Pergamon Press, London 61.

Israël H. (1954) Ann. Geophys. **10**, 93.

Kraakevik J.H. (1958) Recent Advan. Atmos. Elect. Pergamon Press, London 75.

Mauchly S.J. (1923) Terr. Magn. Atmos. Elect. 28, 61.

Mühleisen R. (1956) J. Atmos. Terr. Phys. 8, 146.

Mühleisen R. (1958) Recent Advan Atmos. Elect. Pergamon Press, London 213.

Sagalyn R.C. and Faucher G.A. (1956) Quart. J.R. Met. Soc. 82, 428.

昭和35年 6 月25日　印刷
昭和35年 6 月30日　發行
第11卷　第 4 號

編輯兼發行者　日本地球電氣磁氣學會
代表者　長谷川万吉

印刷者　京都市南區上鳥羽唐戸町63
田中幾治郎

賣捌所　丸善株式会社京都支店
丸善株式會社 東京・大阪・名古屋・仙台・福岡

JOURNAL OF GEOMAGNETISM AND GEOELECTRICITY

Vol. XI No. 4

1960

CONTENTS